

We are IntechOpen, the world's leading publisher of Open Access books Built by scientists, for scientists

6,900

Open access books available

186,000

International authors and editors

200M

Downloads

Our authors are among the

154

Countries delivered to

TOP 1%

most cited scientists

12.2%

Contributors from top 500 universities



WEB OF SCIENCE™

Selection of our books indexed in the Book Citation Index
in Web of Science™ Core Collection (BKCI)

Interested in publishing with us?
Contact book.department@intechopen.com

Numbers displayed above are based on latest data collected.
For more information visit www.intechopen.com



Electrostatic Interactions in Dense DNA Phases and Protein-DNA Complexes

A. G. Cherstvy

*Institute of Complex Systems, ICS-2, Forschungszentrum Jülich, Jülich,
Institute for Physics and Astronomy, University of Potsdam, Potsdam-Golm,
Germany*

1. Introduction¹

Charges. Many constituents of living cells bear large charges on their surfaces. The list includes DNA/RNA nucleic acids [1], cellular lipid membranes [2], DNA-binding [3,4] and architectural [5,6] proteins, natural ion channels [7] and pores, elements of cytoskeleton networks [8], and molecular motors. ES interactions on the nano-scale often dominate the physical forces acting between these components in the last 1-3 nm prior to surface-surface contact, often governing their spontaneous assembly and long-range spatial ordering. There has been a number of excellent reviews covering the general principles of ES effects in nucleic acids [9,10], proteins [11,12,13], lipid membranes [2,14,15], and some other bio-soft-matter systems [16]. Salt- and pH-sensitivity of ES forces provides cells with a useful handle to direct/tune the pathways of many biological processes. Among them are DNA-DNA, protein-DNA [17] and protein-protein ES interactions [18], DNA compactification into higher-order structures [19,20], DNA spooling inside viral shells [21], actin aggregation, RNA folding [10,22], and ion translocation through membrane pores. ES forces modulate structure and control functioning of sub-cellular supra-molecular assemblies [23,24] and can affect cell-cell interactions in tissues [25].

Over the last years, the ES mechanisms of some DNA-related phenomena mentioned above have been developed in our group. General concepts of the PB theory often give a satisfactory physical description of ES properties of molecules in solution and macromolecular complexes. Below, we try to keep the presentation on illustrative level avoiding complicated algebra: all analytical expressions, the details of their derivation, and regimes of applicability can be found in the original papers cited. We rather focus on underlying physical mechanisms, comparing the system behavior under varying conditions. We often treat ES forces in dense, weakly fluctuating structures/complexes, where entropic effects are weak and can be neglected. Because of limited space, we focus on latest ES-motivated developments from other groups, trying to position our research in this context.

¹Abbreviations: ES, electrostatic; HB, hydrogen bond; PE, polyelectrolyte; PB, Poisson-Boltzmann; PEG, polyethylene glycol; DH, Debye-Hückel; EM, electron microscopy; AFM, atomic force microscopy; bp, base pair; kbp, kilo base pair; [DNA], DNA concentration; [salt], salt concentration; ds, double stranded; ss, single stranded; CL, cationic lipids; LC, liquid-crystalline; GNP, gold nano-particle; hom, homologous; NCP, nucleosome core particle; PDB, Protein Data Bank.

Outline. The main aim of this chapter is to provide a review of recent advances in the theory of ES interactions in dense assemblies of DNAs and to discuss some ES aspects of protein-DNA recognition and binding. These subjects have been the main area of my scientific activity in the last several years. ES effects on different levels of DNA organization *in vivo* and *in vitro* are considered below. We overview e.g. the biophysical principles behind DNA-DNA ES interactions, DNA complexation with CL-membranes, DNA condensates, DNA cholesteric phases and touch on DNA spooling inside viruses. For DNA-protein complexes, the effects include ES recognition and binding. For these systems, we develop theoretical frameworks and computational approaches to describe physical-chemical mechanisms of structure formation that allow us later to anticipate some biological consequences.

First, we focus on theoretical concepts used in derivation of the ES interaction potential of two parallel double-helical DNAs immersed in electrolyte solution [9]. The linear PB theory developed for this system [26] accounts for a low-dielectric DNA interior and spiral distribution of negative phosphate charges on DNA periphery. We discuss the regimes of applicability of this linear theory, in application to interaction of DNAs partly neutralized by adsorbed counterions. This theory and its modifications have allowed us to rationalize a number of experimental observations regarding the behavior of DNAs in columnar hexagonal phases (Sec. 2), dense cholesteric DNA assemblies (Sec. 5), the decay length of DNA-DNA ES repulsion in mono-valent salts, the region of DNA-DNA attraction in the presence of multivalent cations (Sec. 2), as well as DNA condensation into toroids (Sec. 3). A separate domain of our research deals with interaction-induced adjustment of DNA helical structure, DNA-DNA sequence recognition and pairing (Sec. 7), as well as DNA-DNA friction (Sec. 8). We also overview DNA melting and hybridization in dense DNA lattices, Sec. 9.

In the second part, we focus on ES recognition between DNA and DNA-binding proteins in their complexes. We propose a model of DNA sequence recognition by relatively small proteins (e.g., transcription factors) based on complementarity of charge patterns on DNA target site and bound protein (Sec. 10). For relatively large proteins, we support the theoretical conclusions by a detailed bioinformatic statistical analysis of charge patterns along interfaces of various protein-DNA complexes, as extracted from their PDB entries. We decipher the reasons why large structural protein-DNA complexes of pro- and eu-karyotic organisms do involve a substantial ES component in their recognition (Sec. 10). On the contrary, DNA recognition by small DNA-binding proteins appears to be ES-non-specific, being likely governed by HB formation.

Every section below starts with a short introduction to the subject, followed by a presentation of basic theoretical concepts and discussion of main results, and it ends with some perspectives for future developments and possible model improvements. The content of this chapter is based on the recent perspective article [27].

2. ES forces between DNA duplexes

Counterion condensation. B-DNA is one of the most highly charged bio-helices, with one elementary charge e_0 per $\approx 1\text{nm}^2$ on the surface at standard pH and physiological [salt]. These charges are the phosphate negative groups located on DNA periphery, forming a duplex with 10-10.5 bp per helical turn of $H \approx 34\text{\AA}$ and non-hydrated DNA radius of $a \approx 9\text{\AA}$. More than $\sim 75\%$ of DNA charge is neutralized by counterions adsorbed onto it from solution. The

Manning theory [28] predicts $\theta_M=76\%$ of charge compensation for mono-valent ($z=1$) and $\theta_M=92\%$ for tri-valent ($z=3$) cations. In the DNA model as a thin long linear PE at vanishing [salt], the neutralization fraction is predicted to be

$$\theta_M = 1 - 1 / (z\xi), \quad (1)$$

where ξ is the ratio of the Bjerrum length ($l_B \approx 7.1 \text{ \AA}$ in water) to the axial PE inter-charge separation, $b \approx 1.7 \text{ \AA}$ for the bare DNA. Recent experiments on DNA translocation through nm-sized solid-state nano-pores enabled measuring the compensation fractions θ [29,30], often in good agreement with the Manning theory.

Cation binding. DNA structure offers well-defined sites for counterion binding. Depending on chemical nature and valence, cations bind in DNA grooves, on DNA strands, or both. The distribution and binding equilibrium of adsorbed cations result in a distinct pattern of charges on DNA surface that, in turn, dictates the properties of DNA-DNA ES forces. It also affects intrinsic DNA helical structure and conformation DNA adopts in solution [31]. ES forces are believed to dominate the interaction of parallel DNAs in the last 20 \AA prior to surface-surface contact, because of still relatively large residual DNA charge density after condensation of counterions.

DNA-DNA hydration force created by overlapping patterns of structured water molecules on DNA surfaces is another alternative [32]. Close similarities in the magnitude and decay length of repulsive forces in the last 1-2 nm prior to the contact measured by osmotic stress technique in simple-salt solutions for DNA, some net-neutral polymers [33,34] and lipid membranes [14,35] favor the hydration force picture. Extreme sensitivity of DNA-DNA forces measured to the chemical nature and valence of cations added, not expected to affect strongly the close-range hydration forces, favors however the ES mechanism of DNA-DNA force generation. In particular, DNA-DNA attraction in the presence of multi-valent cations can be rationalized by our ES models, see below.

The pattern of condensed cations bears some/strong correlations to the helical symmetry of DNA phosphates, forming a "lattice" of alternating positive-negative charges along the DNA axis, Fig. 1. ES forces between these periodic arrays of charges might turn from repulsion to attraction for well-neutralized DNAs. Attractive DNA-DNA forces have been systematically measured by the osmotic stress technique in dense columnar hexagonal DNA assemblies in the presence of some di- and many tri-valent cations at $\approx 1 \text{ nm}$ between the surfaces [36,37], Fig. 2, while purely repulsive forces have been detected with mono-valent salts [38]. The list of DNA condensing agents includes multi-valent cations (cohex³⁺, spermine⁴⁺, spermidine³⁺), some highly positively charged proteins and polypeptides (poly-Lys and poly-Arg, protamines, H1 histones), as well as concentrated solutions of neutral PEG polymers. The latter are excluded from the DNA phase, exerting an external osmotic pressure onto the DNA lattice. Some ions from this list interact with DNA in natural environments, such as spermidine³⁺ present in many bacteria in 1-3 mM concentrations [39], protamines that are abundant in sperm heads, as well as putrescine²⁺ and spermidine³⁺ vital for DNA compaction in some T-even bacterio-phages [40].

Duplex-duplex ES forces. A number of theoretical models have been developed in the last two decades to provide a physical rationale for DNA-DNA attraction, including some recent

advances [41,42]. In one group of models, the spatio-temporal correlations of cations stem from the inherent DNA structure, which render DNA-DNA attraction possible via a “zipper effect”. In other models, beyond the PB limit, the *correlated* fluctuations in the density profiles of condensed cations give rise to attraction [43,44,45], even for DNAs modeled as a uniformly charged PE rods. The period of oscillatory charge density waves on PE surfaces in these models is largely decoupled from intrinsic DNA charge periodicity. To save space, we address the reader to a comprehensive review [9] focused primarily on ES DNA-DNA forces. It provides a broad coverage, physical comparison, and analysis of applicability regimes for various models of PE like-charge attraction. In this chapter, we target primarily *new developments* in the theory of DNA-DNA and DNA-protein ES interactions. DNA-DNA attraction has also been extensively investigated by computer simulations [46,47,48,49], for diverse models for DNA structure, the shape and binding specificity of counterions, as well as for various solvent models implemented.

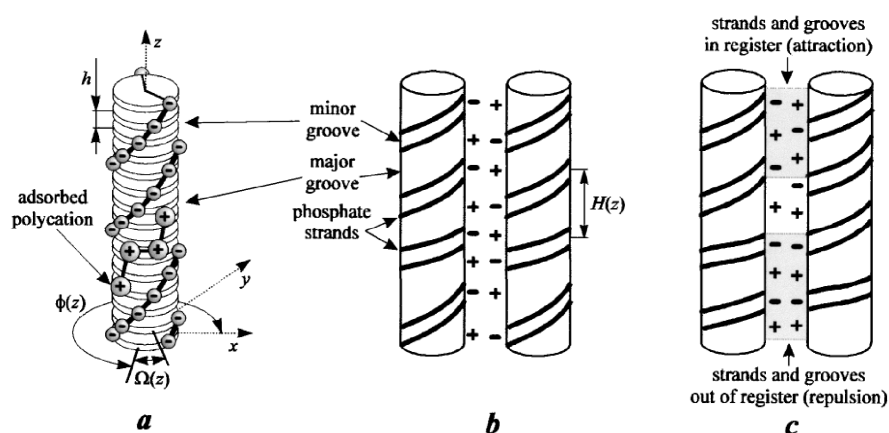


Fig. 1. Schematics of cation-decorated DNA duplexes (a) and interacting hom vs. non-hom sequences (b, c). Positive-negative charge zipper motif that ensures DNA-DNA ES attraction is shown in part (b). The image is reprinted from Ref. [53], subject to APS-2001 Copyright.

The helicity of DNA charges renders the ES potential close to the double helix helically symmetric. When two DNAs approach one another in electrolyte, these helical potential profiles overlap. This affects non-trivially DNA-DNA ES forces, on top of ES repulsion of uniformly charged rods. The exact theory of ES forces between two long parallel double-helical macromolecules was developed in 1997 by A. Kornyshev and S. Leikin [26]. This elegant linear PB theory explicitly accounts for the DNA charge helicity and its low-dielectric hydrophobic core (permittivity of $\epsilon_c \approx 2$).

The model implies two distinct populations of cations around the DNA. The first one is the Manning’s fraction of cations is strongly/irreversibly adsorbed in DNA grooves/strands, while the remaining DNA charge is shielded by electrolyte ions in DH linear manner. DNA ES potential renormalized in this fashion often does not exceed 25 mV, rendering the linear PB model applicable to description of interacting clouds of mobile ions around two partly-neutralized DNAs. Both DNA phosphates and condensed cations in the middle of DNA grooves are modeled below as thin continuous helical lines of charges. Thermal smearing of charge pattern can be incorporated via the Debye-Waller factor [9] that reduces the magnitude of the helical harmonics $a_{1,2}$, see below.

Attraction vs. repulsion. The theory predicts ES attraction of well-neutralized DNAs with the majority of cations adsorbed in the major groove, as pioneered in Ref. [50]. This arrangement of charges facilitates a periodic positive-negative charge alternation along the DNA axis. In physical terms, a DNA-DNA attraction emerges from a zipper-like ES matching of phosphate groups of one DNA with the cations adsorbed in a regular fashion in the grooves of another DNA. Many large or extended multivalent DNA-condensing cations are indeed known to bind preferentially into the major DNA groove, preferred both from interaction and steric point of view. Correlated ES potential alternations thus generate charge interlocking along the DNA-DNA contact and give rise to DNA-DNA ES attraction, see below. The mathematical apparatus used for deriving DNA-DNA forces, ES and chemical features of counterion binding, as well as applicability regimes of this mean-field continuum DH-Bjerrum PB theory are discussed in details in excellent review [9].

Further developments of this theory enabled us to incorporate fine realistic details of DNA structure, such as a discrete nature of adsorbed cations [51] and sequence-specific pattern of the twist angles [52] between the adjacent DNA bps [53]. The models for description of interaction- and T -mediated rearrangements of condensed cations on DNA surfaces [54], torsional flexibility of DNA backbone [55], some soliton-like DNA twist “defects” [56], and DNA helical “straightening” in dense phases [57] have also been developed. ES forces between non-parallel infinitely long [58] and finite-length [59] DNAs were computed and the detailed statistical theory of dense DNA assemblies has been worked out [60].

Basic equations. A number of outcomes of this theory are in quantitative agreement with a number of experimental observations available for DNA assemblies. These include the decay length of DNA-DNA repulsion in simple salt solutions and attraction at $R=28-32\text{\AA}$ in the presence of multivalent cations, Fig. 2. Also, DNA azimuthal frustrations [55,61], DNA straightening [62], and a reduced positional order observed in dense DNA lattices [63] have been rationalized. Recent developments unraveled the effects of DNA thermal undulations [64,65] and have shown that duplex-duplex ES forces might get amplified in DNA columnar phases at finite T , as compared to $T=0$ case. Recently, the implications of binding equilibrium of finite-size ions on DNA-DNA ES forces have been clarified [66]. A number of biological consequences of computed ES duplex-duplex forces were analyzed in excellent recent perspective [67].

DNA-DNA ES interaction energy in electrolyte solution can be approximated as the sum of the first helical interaction harmonics a_n [9]

$$E(R, L) \approx L [a_0(R) - a_1(R) \cos \delta\phi + a_2(R) \cos 2\delta\phi]. \quad (2)$$

These positive coefficients decay nearly exponentially with DNA-DNA separation R , Fig. 3, and their values depend on partitioning of cations on DNA and DNA charge compensation θ as follows [50]

$$a_0(R) = \frac{8\pi^2 \bar{\sigma}^2 a^2}{\varepsilon} \left[\frac{(1-\theta)^2 K_0(\kappa_D R)}{[\kappa a K_1(\kappa a)]^2} - \sum_{n,m=-\infty}^{\infty} \frac{\tilde{f}(n, \theta, f)^2 K_{n-m}^2(\kappa_n R) I_m'(\kappa_n a)}{[\kappa_n a K_n'(\kappa_n a)]^2 K_m'(\kappa_n a)} \right],$$

$$a_{m=1,2}(R) = \frac{16\pi^2 \bar{\sigma}^2 a^2}{\varepsilon} \frac{\tilde{f}(m, \theta, f)^2 K_0(\kappa_m R)}{[\kappa_m a K_m'(\kappa_m a)]^2}. \quad (3)$$

Here, the first term in a_0 describes the ES repulsion between uniformly charged “DNA rods”, that dominates at large R . The second term in a_0 is the image-charge repulsion between the charges on one DNA from image charges (of the same sign) created in a low-dielectric core of another DNA. The duplex-specific DNA-DNA forces are described by $a_{1,2} > 0$ amplitudes. For ideally helical DNAs, the interaction energy scales linearly with the DNA length L , while for randomly-sequenced non-ideal DNA fragments a more intricate dependence arises, see Sec. 7. With the cations adsorbed prevalently in the major groove and at large θ values, the a_1 -term responsible for ES helix-helix attraction grows. Many DNA-condensing multivalent cations are indeed known to adsorb into the major DNA groove.

In these expressions, parameter f controls the partitioning of cations on DNA (at $f=0$ all cations occupy the major groove), $\tilde{f}(n, \theta, f) = f\theta + (-1)^n(1-f)\theta - \cos(n\tilde{\phi}_s)$, $\tilde{\phi}_s \approx 0.4\pi$ is the azimuthal half-width of DNA minor groove, $\bar{\sigma}$ is the surface charge density of DNA phosphates, and $K_n(x)$, $I_n(x)$, $K_n'(x)$, $I_n'(x)$ are the modified Bessel functions of order n and their derivatives.

We note that the decay lengths of $a_{n=1,2}$ harmonics, $1/\kappa_n = 1/\sqrt{\kappa^2 + n^2(2\pi/H)^2}$, is a non-trivial function. Not only it contains the DH screening length in 1:1 solution with [salt]= n_0 , namely $\lambda_D = 1/\kappa = 1/\sqrt{8\pi l_B n_0}$, but also depends on the DNA helical repeat H . We remind here that at physiological conditions $\lambda_D \approx 7-10 \text{ \AA}$, that is $n_0 \sim 0.15-0.1 \text{ M}$ of simple salt.

The image-force repulsion is screened with about half as short decay length, compared to the direct charge-charge repulsion. Effectively, the electric field travels a double distance to image charge. This gives rise to a short-range branch of DNA-DNA ES repulsion at $R < 24 \text{ \AA}$ or so (for typical parameters), see Fig. 2. For intermediate $R = 28-32 \text{ \AA}$, the ES helix-helix attraction overwhelms the short-range image-force repulsion and the direct DH charge repulsion [68]. This renders the net DNA-DNA ES force *attractive* in this range. Typically, at about $R > 35 \text{ \AA}$ the direct DH rod-rod repulsion prevails and DNAs again repel each other.

Note however that the predicted in Fig. 2 short-range repulsion domain is shifted by 3-5 \AA to smaller DNA-DNA distances, as compared to the measured DNA pressure-distance curves. A possible explanation is that the first, tight hydration shell of DNA, not included in the theory, might effectively increase DNA diameter in experiments and thus prevent direct DNA contacts at $R \approx 20 \text{ \AA}$, shifting the energy curves measured towards larger R values.

Another effect is azimuthal frustrations of DNA molecules observed in dense hexagonal DNA lattices [61]. In the theory, they emerge from XY-spin-like $\cos \delta\phi - \cos 2\delta\phi$ dependence of the interaction potential on the mutual DNA rotation angle, $\delta\phi$. Optimization of the interaction energy over all 6 neighboring DNAs on the lattice inevitably “frustrates” the azimuthal order [69]. Frustrated Potts-like states, reminiscent of those for magnetic spin systems, are often preferred for DNA hexagonal lattice in the model [61]. Namely, in the elementary triangle on a lattice, the two differences of the azimuthal DNA angles are

$$\Delta_1 = \pm \arccos \left[1/4 + \sqrt{1 + 2a_1/a_2} / 4 \right], \quad (4)$$

while the third one is 2 times larger [70].

Future challenges. Below, we overview some challenges for the current theory. One of them is water structuring in the hydration shells around the DNA. Namely, the most interesting features of intermolecular forces, including the attraction region, emerge at DNA densities when the shells of “structured waters” on interacting helices can overlap. Also, a distance-dependent “effective” dielectric constant on the length scale of 1-2 water diameters [11], a modified decay of electric fields close to DNA, a finite diameter and precise geometrical form of DNA-condensing cations (e.g., linear flexible polyamines vs. compact cohex^{3+} ions), as well as a limited applicability of the linear PB model, all these points require more accurate theories to be developed close to DNA surface. The solvation of DNA also requires a microscopic treatment of dielectric environments and polarization states upon counterion binding to the DNA. Not only in the theory, these factors also complicate quantitative predictions of DNA-DNA forces by means of computer simulations. Similar complications in description of ES forces on the nano-scale emerge in modeling of DNA-protein, DNA-membrane, as well as protein-protein complexes (discussed in Sec. 10).

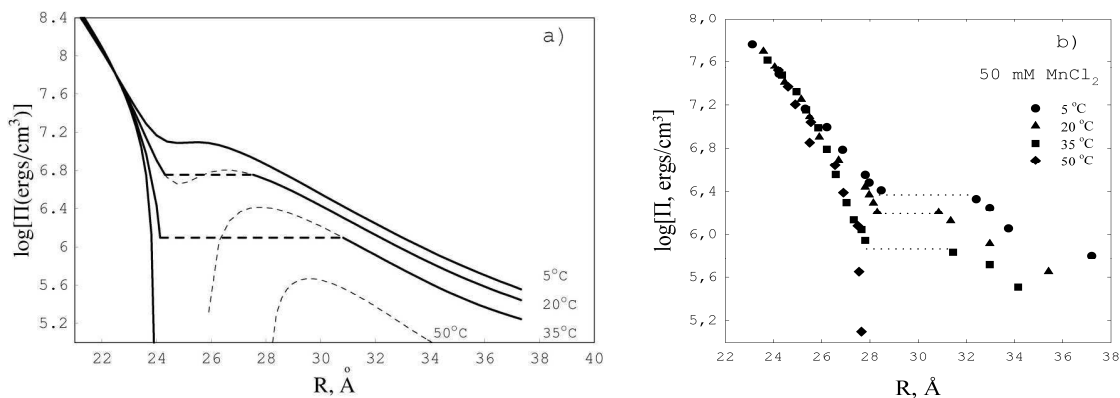


Fig. 2. Theoretically predicted (a) and experimentally measured (b) DNA-DNA forces in dense DNA assemblies at 50 mM MnCl_2 . The region of DNA-DNA attraction at $R=28-32\text{\AA}$ detected in experiments corresponds to a spontaneous shrinkage/collapse of the DNA lattice. No azimuthal frustrations on DNA lattice were considered in the model, i.e. $\cos\delta\phi \equiv 0$ for all DNA pairs. Note that, contrary to majority of di-valent cations, Mn^{2+} and Cd^{2+} are capable of generating DNA-DNA attraction under the osmotic stress of PEG [36]. This technique allows to overcome the long-range DH repulsive branch of the potential and thus enhance the helix-mediated DNA-DNA forces shielded with a shorter screening length, $1/\kappa_1$. Parameters: $\theta = 0.85$, $n_0 = 50$ mM. The figure is reprinted from Ref. [54], subject to ACS-2002 Copyright.

3. DNA toroidal condensation

Structure of toroids. One biological manifestation of cation-mediated DNA-DNA attraction is DNA condensation into compact toroidal structures observed in bacteria, viruses, and sperm cells *in vivo* and studied thoroughly *in vitro* [71]. For instance, some bacteria pack their DNAs into robust toroids to protect the genetic material and minimize the frequency of ds-DNA breaks [72]. These radiation-resistant bacteria retain strongly elevated $[\text{Mn}^{2+}]$ in their cells to regulate packaging of chromatin fibers, via likely attractive DNA-DNA forces [73]. In mammalian sperm cells, very long DNA is condensed with the help of highly basic Arg-rich

proteins protamines into the assembly of interconnected small toroids, as visualized by the AFM technique [74]. DNA compaction inside T5 bacteriophage in the presence of spermine⁴⁺ also exhibits some toroidal-like arrangements for a part of DNA spool, that is likely to optimize the energetics of DNA packing/encapsulation inside viral shells [75,76].

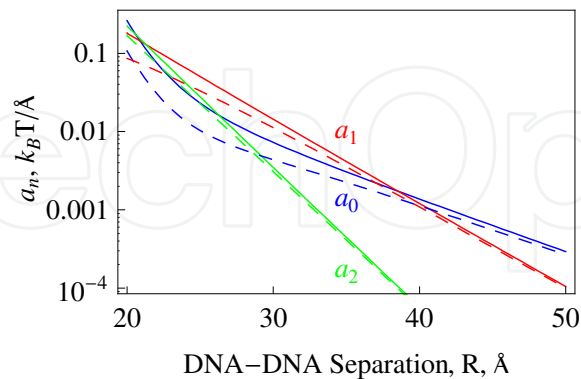


Fig. 3. Dependence of the helical ES harmonics at typical DNA parameters: $\theta = 0.8$, $f=0.3$, $a=9\text{\AA}$, $1/\kappa = 7\text{\AA}$. The solid curves are plotted for two DNAs in solution; the results for dense DNA lattices with the Donnan equilibrium are the dashed curves. In the region of DNA-DNA attraction, the first helical a_1 term dominates the interaction energy. The figure is reprinted from Ref. [27], subject to RCS-2011 Copyright.

In vitro, DNA condensates formed in solutions of cohex^{3+} , as visualized by cryo-EM, often reveal a spool-like DNA organization into tori with $\sim 50\text{ nm}$ outer and $\sim 15\text{ nm}$ inner radii [77], with nearly hexagonal local DNA lattice order, Fig. 4. When several DNA chains comprise a torus, the most frequently encountered condensates contain an optimal number of DNA strands. Often, nearly hexagonal toroidal cross-sections are observed, with a completely filled outer DNA shell, which give the most stable aggregates. Such structures maximize the number of attractive DNA-DNA contacts inside the toroid and minimize the number of (relatively unfavourable) DNA contacts with the solvent. It is important to note that DNA-DNA separations in toroids are often $R \approx 28\text{\AA}$, being in the range of DNA-DNA attraction as measured by the osmotic stress technique and as predicted by the theory of DNA-DNA ES interactions, see Fig. 2.

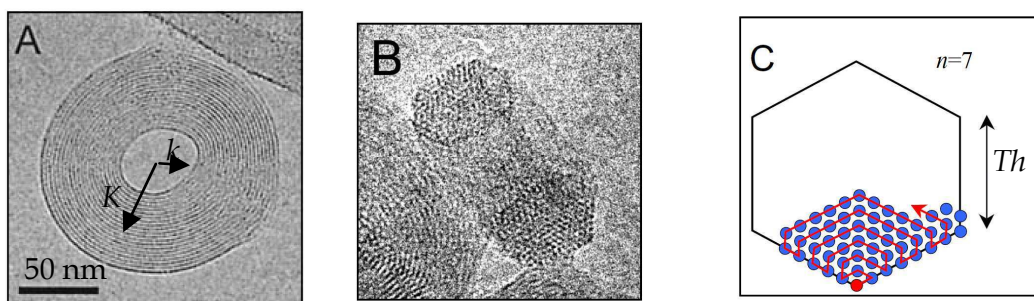


Fig. 4. Cryo-EM images of DNA toroids constructed from 2-3 λ -phage 48.5 kbp long DNAs in 0.2 mM solution of cohex^{3+} (A, B). The mean K and inner k toroidal radii are indicated. One possible model of a defect-free DNA spooling into a torus of generation $n=7$ is shown in part (C). The image is reprinted from Ref. [80], with permission of IOP.

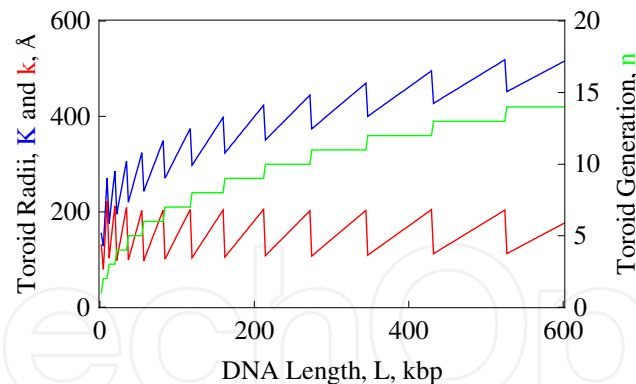


Fig. 5. Radii of DNA toroids of generation n , as obtained at relatively strong DNA-DNA attraction of $E_0 = -0.05k_B T / \text{\AA}$ [80]. The saw-tooth variation of toroid dimensions is due to the growth-by-generation model implemented.

Let us mention one more example of dense DNA assembly, 3D DNA origami structures, where *extremely dense* DNA packing at $R \approx 22\text{-}25\text{\AA}$ is realized [78,79]. A successful assembly necessitates $\sim 10\text{-}20$ mM of MgCl_2 : the divalent cations are likely to reduce the ES repulsion of DNA strands during the assembly process. The latter is driven by the chemical energy of association of complementary ss-DNA fragments into ds-DNA fragments.

Model and outcomes. Utilizing these facts, we constructed a simple model of DNA toroid growth by generations [80]. Due to a finite value of the DNA bending persistence length l_p [81,82], DNA toroids are often preferred over rod-like or (hollow) spherical condensates. During the first stage of compaction, initial DNA circular loop is thermally nucleated and stabilized, with the curvature radius of $\sim l_p$. The growth of DNA toroids is controlled by DNA-DNA attractive ES contacts and by unfavorable energy of DNA elastic deformations.

As the toroidal cross-section increases, the fraction of “missing” DNA-DNA attractive contacts on the toroid periphery progressively decreases (the volume-to-surface ratio grows). This improves the ES attractive energy gain per unit length of DNA compacted, approaching the value one gets for the DNA columnar hexagonal phase, where the pair DNA-DNA interaction is tripled due to six neighboring DNAs. Concurrently, however, DNA wrapping near the inner hole of DNA “donut” costs higher bending energies. The optimal toroidal radius K and thickness M obey the scaling relations $K \propto |E_0|^{-2/5} L^{1/5} l_p^{2/5}$ and $Th \propto |E_0|^{1/5} L^{2/5} l_p^{-1/5}$ [80], as functions of DNA-DNA attraction strength at optimal DNA density $E_0 = E(R_{opt})$ and DNA length L . According to Eqs. 2,3, in the presence of DNA-condensing ions DNA-DNA cohesive energy can reach $E_0 = -(0.01 \div 0.1) k_B T$ per bp along the DNA-DNA contact. It plays the role of the surface tension controlling toroidal dimensions, see Fig. 5. The model reveals that DNA toroids become “fat” as the DNA persistence decreases and DNA-DNA attraction increases: torodial mean radius decreases and thickness grows.

Several theoretical models of DNA toroidal condensation with non-hexagonal and non-circular cross-sections have been proposed in the literature [83,84]. We also want to mention that, although locally the lattice of the wrapped DNA preserves the hexagonal symmetry to make best use of attractive inter-molecular contacts, the path taken by a *continuous* long

DNA upon wrapping into a toroid is still debatable [85,86]. Similar complications emerge for DNA packing inside viral capsids, see Sec. 11.

Perspectives. How stable are DNA toroids? Recent single-molecule optical tweezers manipulation experiments have enabled the researchers to decipher the physical mechanisms behind toroidal stability and gain some insights into DNA condensation dynamics [87]. In particular, a step-wise DNA unwrapping from toroids by applied forces was detected, corresponding to multiple DNA loops released from the condensate. The number of turns released is a function of applied tension of 1-10 pN and of salt-dependent DNA-DNA attraction. Theoretical statistical mechanics models of force-induced DNA unwrapping from DNA “donuts” have also been developed in recent years [88,89].

One intriguing perspective to enrich the morphology of DNA toroids observed in 3D is DNA condensation on positively charged 2D interfaces. Some analysis of deformations of model toroids on wetting/non-wetting surfaces was performed e.g. in Ref. [90], without accounting however for ES DNA-DNA and DNA-surface effects. Indeed, DNA condensation on 2D attractive surfaces (for instance, on CL membranes) is expected to follow different pathways and result in different final morphologies, as compared to DNA aggregation in 3D solutions.

Recently, a coil-globule DNA transition on *unsupported* CL membranes has indeed been reported in Ref. [91]. DNA globules of $\sim 0.1\div 0.4$ μm in size emerge on membranes in 1:1 salt solely due to the presense of mobile positive lipids. They act as counterions for DNA, neutralizing its charge along the DNA-membrane contact. Although a precise morphology of condensates could not be resolved, the hydrodynamic radii of DNA globules were dramatically reduced with the increasing fraction of positive lipids in the membrane. Physically, some patches of positive lipids get bound to DNA deposited on the CL membrane, progressively wrapping around and compacting the DNA coil into a dense globule. The membrane deformations accompanying this process are vital, because *supported* membranes with the same lipid composition do not exhibit a coil-globule DNA transition [92]. Mixing and rearrangement of membrane lipids is also expected to play a role, similarly to the adjustment of lipid charges in DNA complexes with CL membranes, reviewed in the next Section.

4. DNA complexation with cationic lipid membranes

Structure of complexes. Self-assembly of CL membranes with oppositely charged biomacromolecules has been extensively studied experimentally for DNA [93], f-actin [94], microtubules [95], and some filamentous viruses [96]. Dense assemblies of DNA with CL-membranes are promising non-viral transfection vectors for gene therapy applications [97], successfully targeting nowadays several types of cancer [98].

Surface charge density on the CL membranes, $+0.3\div 1$ e_0/nm^2 , is often comparable to that of DNA and thus ES forces dominate their complexation into different phases. Depending on the fraction of cationic lipids, membrane flexibility, and lipid composition, dense well-ordered lamellar L_α^c [93] and inverted-hexagonal H_{II}^c [99] phases are commonly observed in experiment, Fig. 6. The H_{II}^c phases are preferred for artificially soft or intrinsically pre-curved membranes, when a tight cylindrical wrapping of membrane lipids around the DNA takes place. For the lamellar phase, ordered layers of parallel DNAs alternate with CL

membranes (one DNA layer per one membrane), compensating the charge. Note that for f-actin, due to a mismatch in the charge densities, the unit cell of the lamellar stack consists of *two* negatively charged f-actin layers on *both* sides of a CL-membrane.

For DNA-CL complexes, most stable assemblies often occur at the *isoelectric point* of exact charge matching between DNAs and CL membranes [100]. The assembly process is accompanied by almost complete release of condensed counterions from the DNA and membrane surface [101]. Concomitantly, the translational entropy of these “evaporated” counterions is maximized. The DNA-DNA separations measured in DNA-CL complexes are in the range $25\text{\AA} < R < 60\text{\AA}$ and they are often consistent with the picture of counterion-free assemblies.

The ES stabilization mechanism of DNA-CL complexes based on numerical solutions of the *non-linear* PB equation has been established a decade ago, in the model of non-fluctuating rod-like DNAs [102,103,104] and refined for more realistic setups in recent coarse-grained computer simulations [105,106,107]. For the lamellar complexes, a particular attention was paid to ES-driven DNA-mediated adjustment of CL charge density profile [108] and membrane undulations [109] that might help to improve DNA-membrane charge matching.

Model and results. Recently, we developed a similar ES model based on exact solutions of the *linear* PB theory, with the dielectric boundaries (DNA-solvent, membrane-water) and DNA helicity taken explicitly into account [110]. Within this approach, both for L_α^c phase with planar membranes and for H_{II}^c phase with CL membranes wrapped around DNAs, the distribution of ES potential in electrolyte has been calculated. The variation of the complex ES energy was computed as a function of DNA lattice density and CL-fraction on the membrane. Both appear to exhibit a *non-monotonic* behavior, in good agreement with the numerical results of the non-linear model [103]. The energy minimum found from the model roughly corresponds to electro-neutral assemblies [110]. For the lamellar phase, the energy well near the minimum is attributable to ES compressibility of the DNA lattice. A scaling law for its modulus obtained, $B_{comp} \propto 1/R^2$, agrees well with the experimental data [111]. For L_α^c phase, the ES energy of DNA-induced undulatory membrane deformations can be included later on in more elaborate models.

The laws of DNA-DNA ES forces along and across CL membranes were also examined [110]. For instance, for two thin PE rods on a “salty” interface with mobile charges [112] one can get a power-law decay of ES interactions, in contrast to a nearly exponential decay of rod-rod ES screening known in 3D, Fig. 7. Confinement of electrolyte solution between the adjacent membrane layers also modifies the law of screening along the membranes. Namely, for a point charge, an exponential decay of ES potential at small distances d turns into $1/d^3$ power-law at large distances, when the electrolyte in inter-membrane spaces is rendered quasi-2D. The ES forces across a low-dielectric membrane are also renormalized non-trivially [110]. All these features affect the properties of DNA transversal and longitudinal correlations in DNA-CL lamellar phases, as measured in experiments [111].

The theory of duplex-duplex ES interactions enables us also to rationalize [110] the DNA-DNA separations measured in L_α^c phases in the presence of some di-valent cations (Mg^{2+} , Co^{2+} , Ca^{2+}). These are capable of triggering DNA condensation in 2D DNA-membrane system [113], but not in 3D solution. It was observed that at a critical concentration of

divalent salt, $\sim 20\text{-}60\text{ mM}$, the DNA-DNA separations drop abruptly from $\approx 45\text{\AA}$ for nearly electro-neutral complexes down to “universal” DNA compaction density with $R \approx 29\text{\AA}$. Note again that DNA-DNA ES attraction is realized at these R , Fig. 2. Also, for multi-valent spermine⁴⁺ and spermidine³⁺, the DNA-DNA distances in DNA-CL phase appear to be close to those measured in 3D lipid-free DNA condensates [114] and also agree with the predictions of our theory of DNA-DNA ES interactions, Fig. 8. One can conclude that 2D geometry of DNA-CL L_α^c phase facilitates inter-DNA counterion-mediated attraction, rendering ES attraction possible for divalent cations and at DNA charge neutralization fractions measured to be $\theta \approx 0.63$ [113], lower than the Manning estimate of $\theta_M = 0.8\text{-}0.85$.

Applications. A perspective for future research is to enrich the physical understanding of DNA release from sub- μm sized DNA-CL complexes and of their translocation into the cell cytoplasm across negatively charged cell membranes [98,115]. Both processes are necessary for efficient gene delivery, with the transfection efficiency of DNA-CL complexes still remaining low compared to viral-based gene carriers [98]. It is known e.g. that spermine and spermidine not only compactify DNAs in DNA-CL complexes, but can also trigger a DNA release from them via DNA condensation into dense globular/toroidal aggregates in solution. Another pathway for DNA release is designing lipid membrane being unstable in particular cellular cytoplasmatic environments (addition of special “helper” lipids).

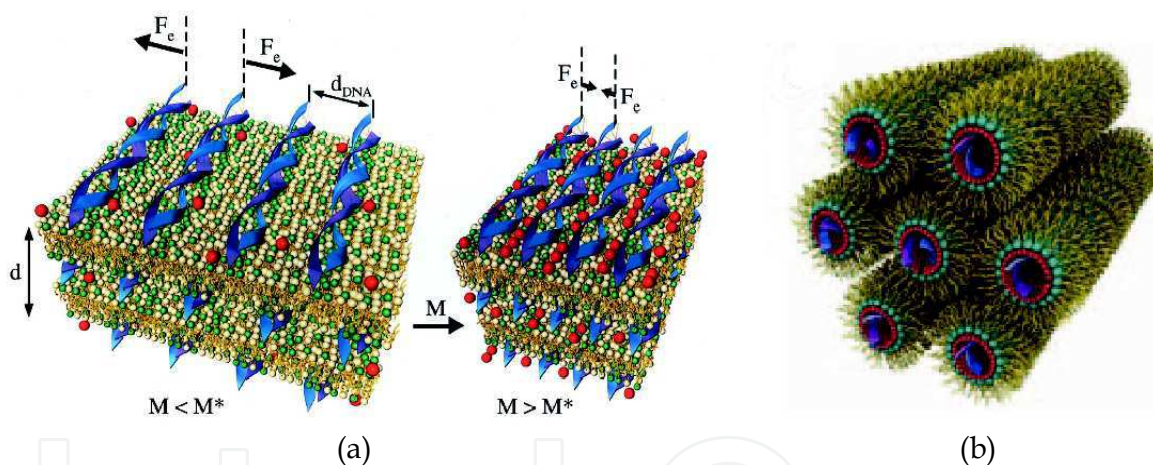


Fig. 6. Schematics of 2D DNA condensation in the lamellar DNA-CL-membrane phase with divalent cations (a). Inverted hexagonal H_{II}^c phase (b). Part a) is reprinted from Ref. [113], copyright 2000-NAS, USA.

$$E_{2D}(R) = k_B T \frac{l_B}{b^2 \kappa_s^2 R^2}$$

$$E_{3D} = 2k_B T \frac{l_B}{b^2} K_0(\kappa R)$$

Fig. 7. Energy density of rod-rod ES repulsions along a “salty” lipid membrane with the inverse Debye length $1/\kappa_s$ and in 3D electrolyte solution.

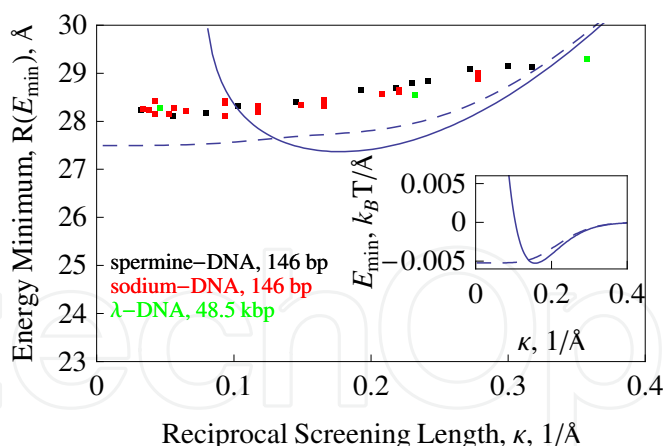


Fig. 8. Optimal DNA-DNA separations measured in dense DNA precipitates with spermine⁴⁺ experimentally [114] (dots) and predicted theoretically [110]. The theory curves with the Donnan saturation (dashed) are more realistic, while the solid curves are for external salt levels also inside the DNA lattice. Multivalent cations only affect the screening in the model: DNA charge fraction ($1-\theta$) stays constant. The inset depicts the ES DNA-DNA energy in the local energy minimum. Parameters: $\theta=80\%$, $f=0.3$.

5. DNA cholesteric phases

Properties of DNA twisted phases. DNA chirality on the nano-scale manifests itself via DNA-DNA interactions in a formation of twisted, ~ 160 - 350 mg/ml dense, LC DNA phases on the micro-scale [116,117]. Cholesteric phases also emerge upon assembly of other bio-helices, e.g., collagen fibers, filamentous viruses [118] and guanosine [119]. Some poly-peptides feature LC phases too. Nature uses the ability of DNA to form chiral phases for packing the genomes in some bacteriophages [120], bacteria [121], and in sperm of many vertebrates [122].

Typically, *left-handed* DNA LC phases are detected, with the cholesteric pitch of $P \sim 1 \div 4 \mu\text{m}$ for ~ 150 bp long nucleosomal DNA fragments [123]. The pitch dependences on the [salt], temperature T , DNA lattice density, and external osmotic stress are however non-trivial functions. For example, the pitch P decreases at higher [NaCl] in the range 0.2-1 M [123]. It reaches $P \sim 20 \mu\text{m}$ for DNA phases with some multivalent cations added [124] and can be reversed by addition of short basic polymers such as poly-Lysine and chitosan.

A number of theories of DNA cholesteric ordering have been developed based on the helical nature of DNA charges [125] in order to rationalize these and many other observations. Some geometrical models imply that right-handed cholesteric pitch is favored by a steric hindrance of DNAs [126], while left-handed phases should originate from ES interactions [127]. Other, purely ES models, treat the DNA charge helicity explicitly and predict a *right-handed* twist direction to be favored for two right-handed DNA duplexes in a close contact [59]. Such twisting direction ensures a more parallel and more ES-beneficial arrangement of negative phosphate strands of one partially neutralized DNA with the "strands" of adsorbed counterions on the neighboring helix. This fact results however in a *right-handed* twist of DNA cholesterics, opposite to a number of experimental observations.

Model and its conclusions. Based on the theory of ES interactions of two skewed DNAs [58], we examined the ES stability of DNA cholesteric phases calculating the strength of DNA-

DNA azimuthal correlations [128], Fig. 9. The DNA “triad model” was implemented, in the ground-state, with no fluctuations, and with a perfect DNA azimuthal register on the lattice [59]. The theory predicts a *non-monotonic* pitch dependence on the DNA density for ≈ 150 bp DNA fragments, in agreement with experiments [123]. Also, the range of DNA densities of $R=35-45\text{\AA}$ predicted is often close to the measured stability domains of DNA cholesterics, Fig. 10. This indicates that long-range ES forces, rather than short-range steric hindrance of the grooved DNA surfaces, are likely to be responsible for DNA LC ordering.

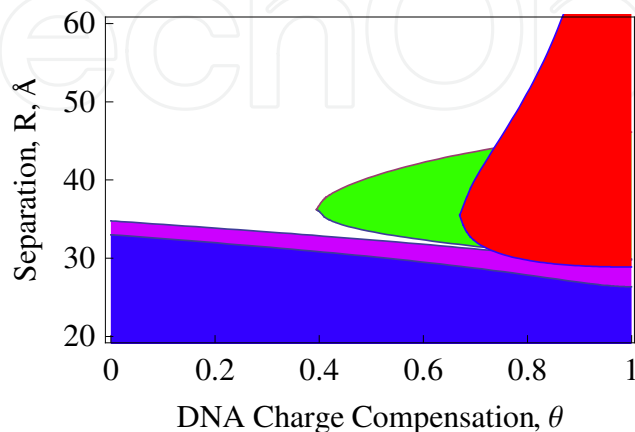


Fig. 9. Stability domains of DNA cholesteric phases. Azimuthal correlations of 150 bp DNAs are strong inside the green domain, as predicted by the theory [59] with the Donnan equilibrium [129]. The energy of azimuthal DNA rotation on the hexagonal lattice exceeds $k_B T$ in the green region. The LC twist elastic constant is $K_{22} < 0$ inside the red domain, the DNA azimuthal rigidity constant is $k_\phi < 0$ for magenta and blue domains (these regions are non-physical). Parameters: $\lambda_D = 7\text{\AA}$, $f=0.3$.

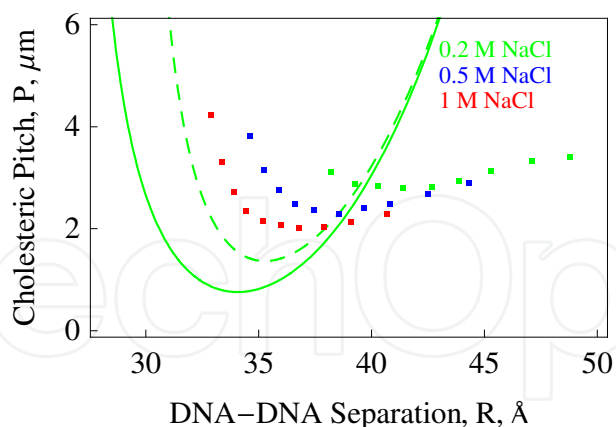


Fig. 10. The value of DNA cholesteric pitch, as calculated from the theory [128] with (dashed) and without (solid curve) the Donnan equilibrium in the DNA lattice. DNA assembly is pressurized to retain a proper [DNA]. Experimental points for DNA LC phases of 146 bp DNAs are taken from Fig. 5a of Ref. [123]. Parameters: $f=0.3$, $\theta=0.65$, and $\lambda_D = 7\text{\AA}$ that corresponds to ~ 0.2 M of NaCl.

Strong DNA-DNA azimuthal correlations are vital for formation of DNA cholesterics. Our ES model [128] predicts that these correlations vanish both at small and large DNA lattice

densities. In the first case, it is due to the decay of DNA-DNA ES interactions, Eq. 3, while in the small- R region the inherent azimuthal *frustrations* of DNA-DNA potential (Eq. 4) destroy DNA orientational order. The existing ES theory of DNA cholesterics [59] has been modified to incorporate the Donnan electro-chemical equilibrium of ions [129] in DNA lattices. This effect appears to be particularly important at low [electrolyte], as follows from the equation for renormalized screening length inside a DNA phase [128]

$$\lambda_D^{Don} \approx \lambda_D \left[1 + \left(\frac{4l_B \lambda_D^2 (1-\theta)}{b(R^2 \sqrt{3} / (2\pi) - a^2)} \right)^2 \right]^{-1/4} \quad (5)$$

Thus, in dense nearly electro-neutral DNA assemblies the DNA lattice density, rather than the bulk [salt], dictates the ionic conditions of solvent between the DNAs, Fig. 11.

Despite a good agreement for the pitch value, the direction of winding of DNA cholesteric layers and the shift of stability domains at different [salt], see Fig. 10, cannot be rationalized by this ES theory in its current form. Right-handed pitch is anticipated at relevant DNA densities of $R=35-45\text{\AA}$, with a possible change to left-handed rotation for very dense DNA packing or atypical counterion patterns on DNA [125]. In the model of dense LC phases with thermally undulating, rather than straight DNAs, a right-to-left pitch inversion might originate from an enhanced contribution of ES image forces. The latter can favor the opposite sense of DNA-DNA crossing, compared to the direct duplex-duplex ES forces. This conjecture requires a detailed future analysis.

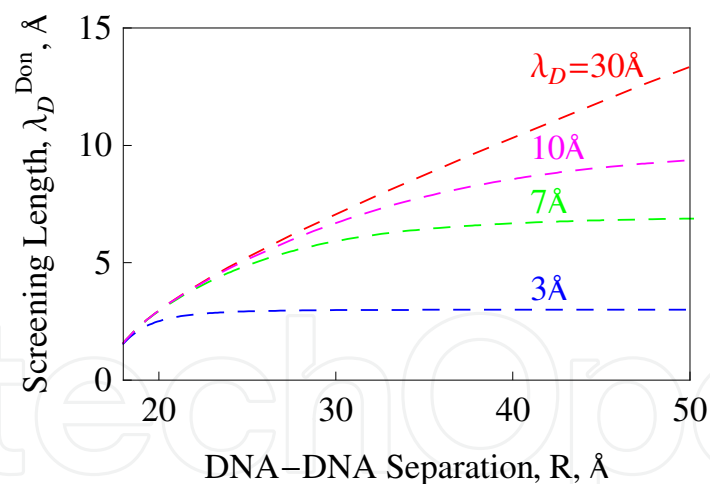


Fig. 11. Effective screening length in dense DNA assemblies for different [salt] in the bulk, as calculated in the cylindrical cell model according to Eq. 5.

Right- and left-handed phases. A major break-through in understanding of LC DNA phases was accomplished recently in Ref. [130]. Namely, an *inversion* of cholesteric handedness in dense LC DNA phases build from $\sim 6\div 20$ bp short DNA fragments has been revealed. Subtle changes in DNA sequence and fragment length were shown to trigger this inversion. These very short DNA fragments stack on each other to form elongated DNAs with a sequence-specific 3D structure [131,132]. For a stacking procedure that generates more regular helical DNA strands, predominantly left-handed LC phases were observed, similarly to those for

≈ 150 bp DNA fragments as well as for kbp-long DNAs. Right-handed phases were observed for short sequences and more azimuthally flexible stacking connections of DNA nano-rods.

The analysis of data (for a variety of stacked DNA oligomers, at different [DNA] controlled by sample dehydration, etc.) enabled the authors to reconcile the results in terms of a single physical parameter [130]. Namely, for DNA lattices with isotropic-nematic phase transition below ≈ 620 mg/ml, the left-handed DNA cholesterics are formed. DNA sequences that experience this transition at larger [DNA], give rise to right-handed LC phases. Thus, for DNA-DNA distances of $R \leq 32 \text{ \AA}$ the right-handed DNA-DNA crossings seem to be favored [133], whereas LC twist is right-handed for DNA fragments shorter than 14 bp [130]. Some of these experimental trends have been supported in recent simulation study [134].

Also, a general trend was detected [130] that shorter DNA oligomers form cholesteric phases with a shorter, sub- μm pitch. This fact is consistent with the ES DNA theory [59] being also akin to $P(L)$ variation for longer DNAs [135]. For shortest DNAs, the pitch of $\sim 0.3 \mu\text{m}$ was detected, much smaller than 2-4 μm for ~ 150 bp fragments. Systematic analysis of [salt] and T -dependence revealed also several unexplained features. Some sequences exhibit e.g. a pitch reversal at [DNA] of 620 mg/ml. Also, for the majority of DNA oligomers, the pitch increases with T indicating an unwinding of cholesteric structures, regardless of their handedness. For many sequences, the pitch was almost insensitive to [salt], contrary to a strong $P([\text{salt}])$ dependence measured for ≈ 150 bp DNAs [123]. All in all, this detailed investigation of twisted phases of stacked nano-DNAs [130] has enriched enormously a widely accepted view of “left-handed-only” DNA cholesterics, challenging future theoretical investigations of DNA twisted phases.

6. DNA-mediated ES interactions of nucleosomes

DNA compaction. NCP-mediated DNA compaction in eukaryotic chromosomes ensures enormous compactification “power” often required to pack meter-long genomes in $\sim \mu\text{m}$ -sized cell nuclei [19]. This process takes place on several hierarchical levels, with the initial step being the 30-nm chromatin fiber, an organized array of NCPs connected by a continuous DNA. Structure of this fiber is sensitive to many biological factors such as ionic environment, DNA linker length, concentration of H1 linker histones [136], charge state of histone tails, etc. It is still debated what conditions favor solenoidal [137] vs. zig-zag [138] arrangements of NCPs in chromatin fibers. *In vitro*, recent fiber reconstitution experiments provided a great deal of information about inherent stability, NCP linear density, and diameter of chromatin fibers for various lengths of DNA linker [139]. The energetics of DNA-histone [140], H1-NCP, and NCP-NCP [141] contacts is vital for physical understanding of chromatin fiber structure, stability and functioning.

Similarly to unwrapping of DNA toroids that enabled to rationalize their stability [87], recent measurements of force-induced stretching of chromatin fibers revealed the NCP-NCP cohesive energies of ≈ 3.4 [142] and later of $\approx 14 k_B T$ [143], depending on concentrations of mono- and di-valent cations. Ionic conditions dramatically influence also the forces required to disrupt the NCP-NCP contacts in chromatin fibers (typically ~ 2 -5 pN) and to induce a DNA unwrapping from NCPs (~ 6 -20 pN). These cohesive energies guarantee the fiber stability, but also allow for some “unwrapping plasticity” and “breathing dynamics” of complexed NCPs, both required for DNA transcription to take place.

Top-to-bottom NCP-NCP stacking contacts are likely to be hydrophobic, governing formation of NCP columns in NCP crystals, semi-crystalline NCP phases, NCP multi-layered helices, etc. The side-to-side contacts, with the wrapped DNAs being often in close contact, on the contrary, are likely ES in nature, Fig. 12. Close similarities in condensation and re-solubilization of DNAs and NCPs support this statement. These [salt]-dependent ES contacts control the formation of mesophases of isolated NCPs *in vitro* [144].

The stability of dense NCP phases is controlled by side-to-side DNA-mediated NCP-NCP contacts. In these phases, the DNAs on contacting NCPs are separated by only 5-15Å of electrolyte, that is typically within one Debye length λ_D . For the NCP bilayer phase [145], the NCPs are oriented in columns so that their dyad axes point on average perpendicular to the bilayer plane and the NCP sides with 2 DNA turns are buried inside the bilayer. The NCP azimuthal orientations are frustrated and distributed within $\pm\approx 35^\circ$ from this preferred direction [145]. Stronger DNA-mediated contacts of NCPs *inside* the bilayer govern its formation, being likely responsible for peculiar NCP azimuthal frustrations observed.

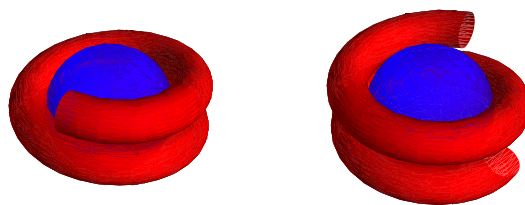


Fig. 12. Schematics of inter-nucleosomal interactions, with the positive histone cores shown in blue and super-helically wrapped DNA depicted in red. This in-plane orientation of NCPs corresponds to a 2:2 DNA-DNA contact.

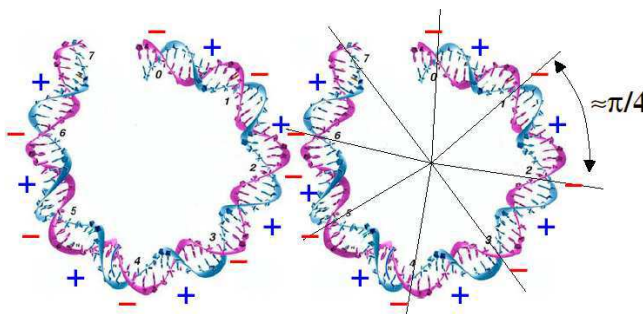


Fig. 13. Schematics of NCP-NCP interactions modulated by charge periodicity of wrapped DNA. Zipper-like charge motif is viewed along the DNA superhelical axis, for a referential counterion adsorption into the DNA major groove. Data of NCP 1aoi.pdb structure was used. The image is reproduced from [147] with permission of IOP.

Model of inter-NCP ES forces. Crystal structures of NCPs show ≈ 8 full DNA helical turns per one superhelical turn of the wrapped DNA. DNA turns in NCPs are separated by the same “magic” $R \approx 25\text{\AA}$. At these distances parallel DNAs attract each other in dense assemblies with MnCl_2 , Fig. 2, and they are close to equilibrium separations in DNA toroids, Sec. 3. An important ingredient of the model is the structural fact that two turns of DNA wrapped in NCPs bear a strong positional *register* forming a “super-groove” [146]. As we have seen in Sec. 2, the DNA in electrolyte solution exhibits a distinct pattern of alternating charges along

its axis (negative phosphates vs. positive condensed cations). Thus, this positive/negative DNA *charge zipper* along the side-to-side contact of two in-plane NCPs modulates their azimuthal interactions with the period of $\approx \pi / 4$, see Fig. 13.

For in-plane NCPs with parallel axes, we demonstrated that this azimuthal modulation gives rise to quantization of NCP orientations in nucleosomal bilayers with periodicity of $\approx 45^\circ$ [147]. Azimuthal optimization of side-to-side contacts of NCPs in bilayers resembles the azimuthal adaptation of short DNA fragments in columns of nano-DNAs in the cholesteric phases, Sec. 5. Both effects likely originate from DNA helix-helix ES interactions.

Generally speaking, the DNA contribution to NCP-NCP ES energy is 4 times stronger for the NCP sides with 2 DNA turns as compared to the NCP sides with only 1 DNA turn. For the in-plane NCPs, we calculated the ES forces and attraction-repulsion phase diagram, see Fig. 14. We implemented a simple model of ES double-layer repulsion for the histone cores, modeled as uniformly charged spheres with charge Q . For the DNA part, the Derjaguin approximation was used to compute the ES forces between the bent DNA duplexes, interacting locally according to Eqs. 2,3.

For a typical histone charge $Q=+220e_0$, at physiological salt conditions, the model predicts for the 2:2 DNA-DNA contacts the maximal NCP-NCP attractive forces of 2 pN for $\theta = 0.8$, $f=0.3$ (typical parameters used in the theory, as in Fig. 14). The NCP-NCP attraction reaches 8 pN at $\theta = 0.9$, $f=0.3$ (better DNA charge neutralization), and even 60 pN at $\theta = 0.8$, $f=0$ (stronger DNA-DNA attraction due to binding of cations into the major groove [50]). As the histone positive charge grows, the DH repulsion of NCP cores overwhelms the DNA-DNA ES attraction. Thus, at larger Q/e_0 values, the NCP-NCP attraction region at 25-35Å between DNA fragments along the NCP-NCP contact disappears, see the inset in Fig. 14.

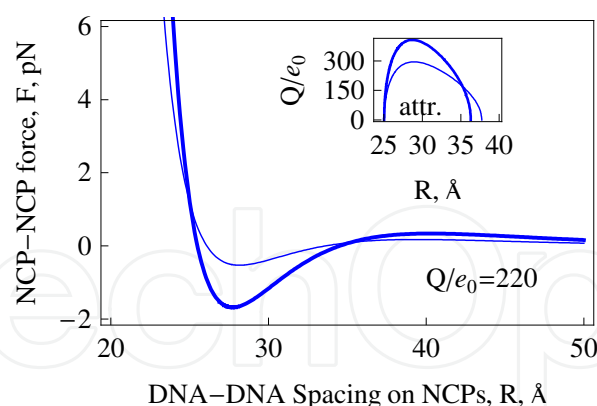


Fig. 14. ES force between two NCPs with parallel axes. Optimal NCP azimuthal alignment is assumed: DNA-DNA attraction. Here R is the distance between DNA axes on NCPs contacting side-to-side ($R=2a=18\text{\AA}$ is direct DNA-DNA contact). Thick and thin curves are for 2:2 and 1:1 DNA-DNA contacts, respectively. ES NCP-NCP attraction-repulsion diagram is shown in the inset. Parameters: $\theta = 0.8$, $f = 0.3$, $1/\kappa = 7\text{\AA}$.

DNA-mediated ES attractions of 2:2 vs. 1:1 DNA sides of NCPs are likely to trigger the bilayer formation and NCP azimuthal frustrations. Another possibility is that histone tails bridge neighboring NCPs in bilayers in azimuthally dependent manner [145]. At typical conditions,

the range of DNA-mediated and tails-mediated NCP-NCP interactions might indeed overlap, being thus hard to distinguish. And, the histone tails also follow the symmetry of DNA in NCPs, protruding into solution through the aligned minor grooves of the DNA superhelix.

To reconcile numerous observations for semi-dense NCP phases, NCP crystals, and chromatin fibers, a rigorous theory of ES NCP-NCP interactions is to be developed in the future. For arbitrary orientations of NCPs in space, one has to take into account the helicity of DNA charges, a heterogeneous distribution of histone charges on the side and top/bottom NCP surfaces, a low-dielectric core of histones and the DNA, DH ES screening by electrolyte, and the counterion separation-dependent condensation. All these effects make such a theory a formidable problem of the mathematical physics, even within the linear PB theory.

7. Homology recognition of DNA sequences

DNA structure. So far, ES forces between ideally-helical parallel or skewed DNAs were described. The locality of intermolecular potential gives rise to the same ES energies for DNA fragments hom in sequence, but not ideally helical. Below, the sequence effects on DNA-DNA ES forces are overviewed. To save space, we dwell here on several subjects only, addressing the reader to an excellent recent perspective [67] that covers all aspects of ES DNA-DNA recognition and also suggests biological phenomena where it is of potential importance. One immediate application of the theory is to provide a physical rationale [148] for recognition and pairing of hom genes on genomic ds-DNAs [149,150] during cell division.

The physical mechanism of ES DNA-DNA sequence recognition was pioneered in Ref. [53] for parallel torsionally rigid DNAs and later extended for duplexes with a realistic value of torsional rigidity [55]. The ES recognition emerges in the model solely due to the inherent bp-specific non-idealities of DNA helix, as extracted from the analysis of structural data on DNA-DNA and DNA-protein crystals [151]. In particular, the DNA bp twist angles are known to exhibit a strong variation [52,152] fluctuating in a range of 28-40° that gives rise to $\approx 36 \pm 5^\circ$ angle deviations.

In the theory, these variations for a randomly-sequenced DNA form the *helical coherence length* that is $\lambda_c = H / (10 \Delta\Omega^2) \approx 45$ nm at a typical value $\Delta\Omega \approx 5^\circ$. This length controls the degree of DNA non-idealities that strongly affect DNA-DNA ES forces. A finite DNA twist persistence length $l_{tw} \approx 75$ nm allows for some interaction-induced DNA torsional adjustments to take place. These restore to some extent the DNA helical register along such sequence-unrelated DNA fragments [55].

Results. We define below the recognition energy $\Delta E(L)$ as the difference in ES interaction energy for hom and randomly sequenced DNA fragments of length L . For torsionally *rigid* DNA fragments, with azimuthally free ends, in the leading a_1 -approximation we get [53,70] $\Delta E(L) \approx a_1 \lambda_c \left[L / \lambda_c + 2e^{-L/(2\lambda_c)} - 2 \right]$. In the opposite limit of torsionally adaptable, *very soft* DNA duplexes, the recognition is also described by a simple formula [70] $\Delta E(L) \approx a_1 \frac{\lambda_t}{2\lambda_c} \left[L - \frac{\lambda_t}{2} (1 - e^{-2L/\lambda_t}) \right]$, where $\lambda_t(R) = \sqrt{C / [2a_1(R)]}$ is the R -dependent DNA torsional adaptation length. For a standard value of DNA twist modulus, $C = 750 k_B T \text{ \AA}$, the exact analytical expressions for $\Delta E(L)$ are however quite cumbersome [55]. Roughly, at

relevant parameters, the theory predicts that two DNA fragments with unrelated sequences attract each other nearly half as strong as two hom DNA sequences do, see Fig. 15a.

The ES recognition energy predicted grows linearly with the length of DNAs in contact [55], resembling thereby some properties of DNA hom recombination *in vitro* in the absence of specific DNA-pairing proteins, Fig. 15c. The recognition energy exceeds several $k_B T$ for closely aligned DNA fragments of ~ 200 -500 bp in length. This energy is large enough to ensure a stable pairing of hom DNA segments at ambient temperature. It can also be sufficient to trigger unpairing of DNA single strands, required as initial step of hom recombination.

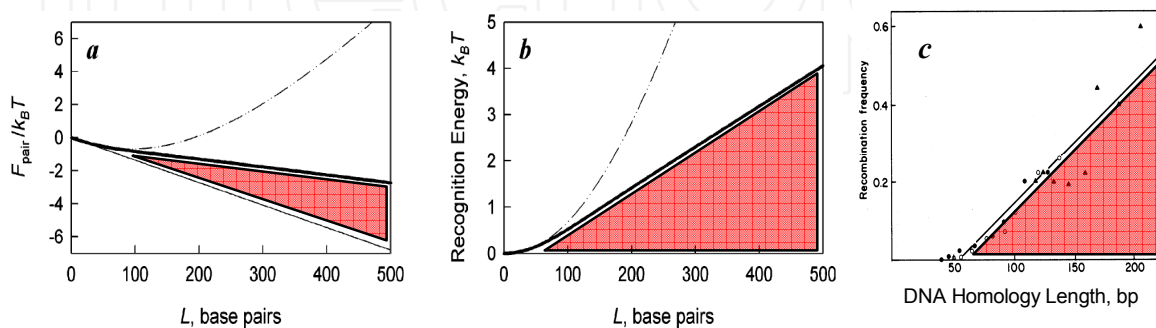


Fig. 15. a) Computed ES interaction energy in a pair of hom DNAs (thin), randomly-sequenced torsionally rigid DNA fragments (dot-dashed), and randomly-sequenced DNA fragments with a realistic twist rigidity C (solid curve). b) The corresponding DNA-DNA ES recognition energy. Parameters: $R=30\text{\AA}$, $\lambda_D=7\text{\AA}$, $\theta=0.8$, $f=0.3$, $l_{tw} \approx 750\text{\AA}$. c) Measured frequency of hom recombination events in T4 phage [153]. It shows a minimal length of DNA homology of ≈ 50 bp necessary for recombination to start and a linear growth of frequency with DNA homology length. This resembles a linear growth of the recognition energy for long DNA sequences in b). The images are reprinted from Ref. [55] with permission of the ACS and from Ref. [153] with permission of Elsevier.

For pulling two ds DNAs one over another, with the hom bp domains in them, the energy well for ES recognition has recently been theoretically computed [148]. For very closely juxtaposed DNAs at $R=30\text{\AA}$, the recognition energies of up to 5-10 $k_B T$ and pinning forces near the bottom of the well of ~ 2 pN were predicted for typical DNA parameters, Fig. 16.

Sequence-specific DNA recognition and pairing for intact duplexes was indeed observed for yeast hom DNA chromosomal loci, in the absence of any *recA*-family proteins [154]. It was attributed to some sequence-specific DNA-DNA forces, capable of initiating and maintaining a proximity of hom DNA fragments. Recently, several experimental techniques have been utilized to elucidate the properties of DNA-DNA hom pairing in denser arrangements [155,156,157]. In one study on dense DNA cholesteric spherulites, the segregation of ~ 300 bp DNA fragments with identical bp sequences into separate LC populations has been clearly identified [156] (telepathic DNAs). This offered a first proof of direct DNA-DNA recognition, based solely on DNA bp sequence information. The effect was attributed to more favorable ES interactions of hom DNA fragments as compared to non-related ones. ES DNA-DNA bp-specific forces [148], are likely to be responsible for the observed segregation of hom sequences at these relatively high [DNA] corresponding to $R=32\div 40\text{\AA}$.

In another study, single-molecule magnetic tweezers measurements revealed an efficient sequence-specific pairing of λ -ds-DNAs with hom regions longer than ~ 5 kbp, at [salt] and [DNA] close to those *in vivo* [157]. The paired structures of hom DNAs were sheared by $F \approx 10$ -20 pN forces and pairing was more profound in the presence of MgCl_2 , indicative of ES nature of this effect. Some other properties, such as a strong enhancement of pairing efficiency with [simple salt] up to 1 M as well as a non-monotonic T -dependence favored however rather some non-Coulomb origin of pairing forces. Also, in experiments, the precision of hom DNA-DNA register along the DNA pair measured is often ~ 2 -5 μm , much larger than the width of the recognition energy well in the model, $\sim \lambda_c \approx 10 \div 50$ nm [148], see Fig. 16. This width in experiments is also independent on the length of the paired hom DNA segments. Future developments of this highly promising technique might provide more information about the axial proximity of paired hom DNA fragments and thus enable us to estimate the effective “range of action” of these sequence-specific DNA-DNA forces.

To summarize, we do believe that helix-specific ES forces can govern DNA-DNA sequence recognition in dense DNA phases [156], at high [DNA] and suppressed DNA fluctuations. DNA-DNA homology associations *in vivo* are however often maintained at much larger separations and take place between fluctuating DNAs [158]. The pairing remains efficient at DNA-DNA distances of 100-300 nm, much longer than the Debye screening length that limits the action radius of ES forces. DNA-DNA hom pairing should thus also involve a recognition mechanism other than the direct ES forces [159], probably recruiting proteins for protein-mediated homology-specific DNA-DNA contacts.

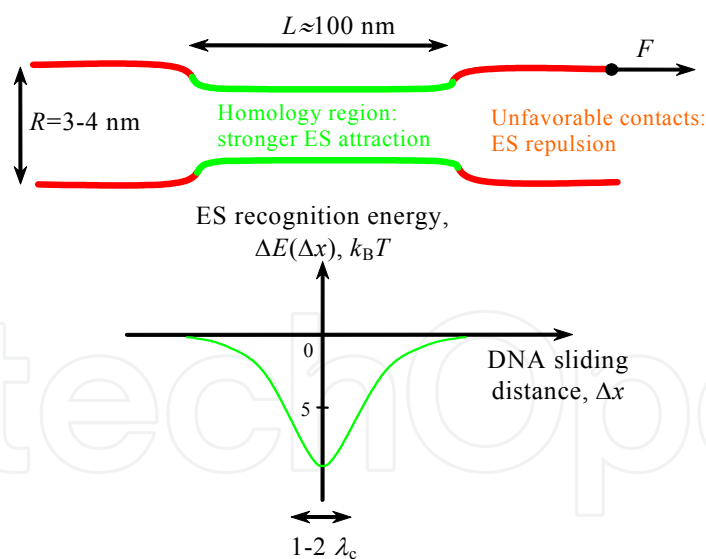


Fig. 16. Pictorial shape of the recognition energy well for sliding of two DNAs with a hom domain, as obtained from Eq. (1) of Ref. [148] for rigid DNAs. DNA hom segments are marked in green; non-hom sections are in red. Hom fragments are pinned near the well bottom by a stronger ES attraction, relative to the rest of DNA. Parameters: $\lambda_c = 100$ Å, $R = 30$ Å, $\theta = 0.8$, $f = 0.3$, $1/\kappa = 7$ Å that give $a_1 \approx 0.015$ $k_B T / \text{Å}$. The helical coherence length for DNAs in solutions and wet fibers $\lambda_c = 10$ -20 nm, is much shorter than in DNA crystals, $\lambda_c = 50$ -100 nm [57], where the helices are “straighten” by mutual interactions.

8. Close-range DNA-DNA ES friction

Modern nano-tribology applications necessitate a detailed understanding of frictional forces between bio-molecules on the nano-scale [160,161]. For DNA, recent advances in single-molecule manipulation techniques has allowed measuring the forces required to pull one DNA over another one in a tight superhelical DNA ply, the dual optical trap. Tight winding of two DNAs in the ply can facilitate their interactions [162]. Upon shearing the ply, in the presence of DNA-associated DNA-bridging H-NS proteins, the frictional forces up to ~25 pN were detected [163]. They emerge from disruption of DNA-protein-DNA bridges formed every several H along the ply. Also, when some small proteins bind to the ds-DNA and sterically impede DNA pulling, the friction of ~2-5 pN was detected. For the “bare” DNAs, one could expect that inherent DNA helicity on $H=3.4$ nm scale might itself generate some friction. With the same apparatus, no measurable friction was detected however [164]: surprisingly, the forces remained <1 pN, independently on the length of DNA ply, DNA pulling speed, and the presence of DNA-condensing (spermine⁴⁺) cations. Diameters of DNA plectonemes in experiments were estimated to be ~5-10 nm.

In this and the next Section, we discuss two manifestations of sequence-dependent DNA-DNA interactions considered in Sec. 7, for DNA-DNA friction and DNA melting. Using the theory of DNA-DNA ES forces, Sec. 2, we examined different regimes for DNA-DNA nano-friction depending on the character of DNA sequence [165]. For ideally helical non-fluctuating and closely juxtaposed DNAs, the ES friction emerges due to spatial correlations of ES potential along DNA surfaces, Fig. 17. At relevant [salt], these correlations are only pronounced in the first ~10Å from the DNA surface. ES frictional force in this regime oscillates with the period of $H=3.4$ nm, while its magnitude grows linearly with the length of DNA L . Namely, the force of static friction is $F_{fr} = 2\pi a_1 L / H$. For slow DNA pulling, this gives rise to a *stick-slip motion* on the nano-scale [165]. The friction however remains rather low. Even for very tight DNA plies, with thickness of ~40 Å and parameters favoring DNA-DNA attraction (large a_1), the upper estimate for frictional force in a ply of $N = L / H = 10$ DNA turns long is as small as ≈ 4 pN.

Several effects are likely to reduce this upper limit. It is the case for pulling non-ideally helical DNAs (random bp sequence). For such DNAs, the “corrugations” in DNA helical structure progressively accumulate with the length [53] and ES potential variations along the DNA-DNA contact become de-correlated, as discussed in Sec. 7. This, in turn, strongly impedes ES friction that attains in this limit an exponential decay with the pulling distance of one DNA with respect to another one. As ES forces decay exponentially with R , it is not surprising that for DNA plies that are typically much thicker than 40Å, being formed by fluctuating DNAs with quasi-random sequences, no measurable friction has been detected in DNA-pulling experiments [164].

The situation might however change, when tight DNA plies are realized (by larger static stretching forces applied to DNA ends) and for DNA sequences with some degree of bp homology. One important example is DNAs fragments artificially designed to contain *repetitive bp hom blocks* with the length of ~50-300 bp. Then, one could expect some homology-mediated DNA pinning events upon mutual pulling of DNAs at the positions when these hom blocks on two DNAs overlap. The theory predicts [148] that these pinned states have a measurable

half-width of $\sim \lambda_c$, see Fig. 16. Therefore, every bp-block pins with its hom partner on another DNA and their action along the chain accumulates enhancing the magnitude of DNA-DNA friction (i.e., the force to remove the system from the favorable state of fully overlapping hom blocks increases). This renders the detection of such pinning mode amenable for the current experimental technique [164] with the resolution of several repeats H . We would like to encourage the experimental groups to check whether such blocky-homologous DNAs experience different frictional forces in tight DNA plies. On the contrary, the resolution of at least $H/2$ is necessary to probe the predicted above ES DNA-DNA friction F_{fr} on the scale of DNA helicity of 3.4 nm.

One potential application of DNA-DNA friction discussed is on DNA ejection from ds-DNA phages, when densely packed DNA strands have to slide passing each other upon reorganization of DNA layers inside the capsid during DNA compactification and ejection.

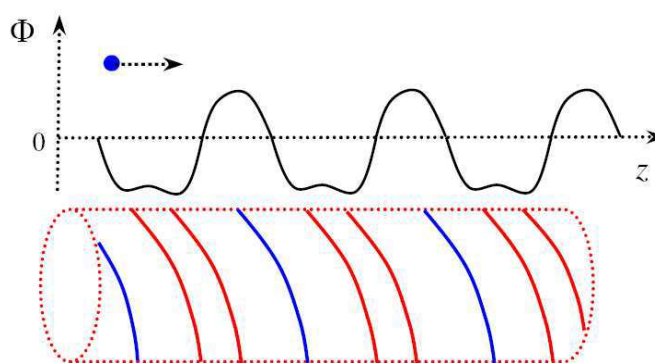


Fig. 17. Schematics of ES potential barriers $\Phi(z)$ near the B-DNA surface [166]. Negative DNA phosphate strands are shown in red, the counterions adsorbed in the DNA major groove are depicted as blue helices.

9. DNA melting in columnar assemblies

Upon heating up to $\approx 50-100^\circ\text{C}$, depending on GC-content and bp sequence, DNAs melt cooperatively in solution and their strands separate. Being thoroughly studied at low [DNA] [167,168,169], DNA melting in dense assemblies, when intermolecular forces become comparable to the internal DNA binding energies, remains not completely understood. The effects of DNA sequence on DNA melting in hexagonal assemblies are discussed below, within a simple thermo-dynamical model [170]. Namely, we predict that melting of hom DNAs is inhibited, while ds-to-ss DNA transition for un-related DNA sequences is facilitated.

In particular, it is straightforward to show that under the conditions favoring duplex-duplex ES attraction, ideally helical hom DNAs melt at higher T due to a stabilization of DNA helical regions by mutual interactions. For hom DNA fragments, the model predicts a rise of the melting temperature T_m (typically by $3-10^\circ$ at $R=23-28\text{\AA}$ between DNAs in the assembly) and more cooperative DNA melting transitions. The shift of T_m scales with the strength of attraction, namely $\Delta T_m \propto 3|a_0 - a_1|$. It can thus be controlled in future melting experiments in dense DNA phases via addition of attraction-mediating cations, e.g., counterions with enhanced binding into the DNA major groove and propensity to induce DNA aggregation.

Also, the model predicts a change in the character of the melting transition, from the second to the first order at a critical strength of DNA-DNA ES attraction [170], Fig. 18. Then, at the melting point the fraction of ds helical DNA regions exhibits a discontinuous change. At the isotropic-cholesteric DNA transition, at moderate [DNA] \approx 100-150 mg/ml, a clear indication of such T_m jumps by several degrees was observed and quantified already long ago [171].

Recently, for dense aggregates of 10-50 nm GNPs linked by short DNA fragments [172] an extremely sharp DNA melting transition has been monitored, with a width of transition of 1-2°C, much smaller than \sim 10-20°C for melting of the same DNA in solution. This *enhanced cooperativity* of melting was attributed to short-range DNA-DNA interactions that trigger an accumulation of ions from electrolyte in the overlapping double layers around DNAs [173], in a Donnan-like fashion. For dense DNA bundles connecting DNA-functionalized GNPs [174], with DNA-DNA distances $R = 25 - 40 \text{ \AA}$, a higher local [salt] near DNAs are realized, which in turn tends to stabilize the ds-DNA state and increase T_m . The effective growth of T_m at these [DNA] was calculated to be 5-20° [173], based on a linear increase of T_m with $\log[\text{salt}]$ [172]. Once the melting of DNA bundle connecting GNPs starts, it progressively releases the excess counterions thus destabilizing the remaining ds DNA links. This might cause a sharp melting of the entire GNPs-DNAs assembly, as detected in experiments [172].

Our DNA melting model for dense aggregates of identical DNA helices [170] does account for the Donnan equilibrium in the DNA lattice, that would give a corresponding [salt]-induced rise of T_m [175]. The additional T_m shifts illustrated in Fig. 18 are however solely due to ES attraction of hom ds DNAs that appears also to be capable of inducing abrupt changes in the average DNA helicity.

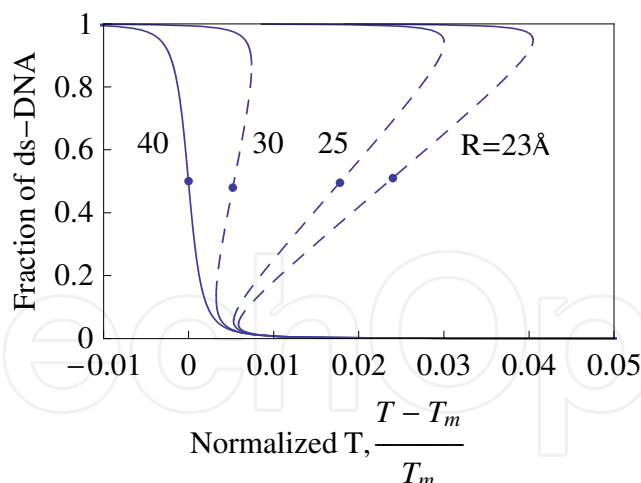


Fig. 18. Melting profiles predicted for long hom DNAs in the hexagonal assembly at varying DNA density. Dots on the curves indicate the T_m at which an abrupt change in DNA helicity occurs (between the stable branches of the melting curve, due to a Z-shaped DNA melting isotherm realized at large enough DNA-DNA attraction). Parameters are the same as in Fig. 16. The figure is reprinted from [170], subject to ACS-2005 Copyright.

For ds DNA random in sequence, pressurized externally to form dense assemblies, one can expect on the contrary a destabilization of the helical state [170] by DNA-DNA ES length-

dependent interactions overviewed in Sec. 7. The physical mechanism here is more formidable. Namely, the melted ss DNA domains/bubbles are going to be created on ds DNAs to optimize *unfavorable ES repulsions* predicted for bp-random DNA stretches longer than $1-2 \lambda_c$ [55], see the dot-dashed curve in Fig. 15a. The melting transition becomes less cooperative in this case. An experimental support of some of these findings might come from T_m -measurements in strongly confined wet DNA films [176].

Lastly, recently, I contributed to the invention of a method and apparatus to detect DNA melting and hybridization events with the help of bio-nano-sensors functionalized with dense DNA lattices. The situations of direct DNA attachment to the sensor surface and DNA deposition via GNPs have been considered. For the former, the sensor signals recorded upon DNA hybridization were rationalized [177] based on the theoretical model of redistribution of mobile counterions in spaces between DNAs (Donnan equilibrium). For GNP-DNA deposition, a more detailed ES screening model was developed [178]. This second detection setup allowed us to systematically monitor the change in the sensor response depending on mismatches in bp composition between probe and target ss DNA sequences. Such sensitivity is vital for a number of biological and biomedical applications involving detection of DNA sequences. This technique might also enable a detection of sequence-specific effects in DNA melting predicted above.

10. DNA-protein ES recognition: Models and reality

Protein-DNA recognition. Despite enormous experimental and theoretical efforts, the recognition laws of DNA-binding proteins and their cognate sites on ds DNA remain quite obscure. Geometric shape complementarity of proteins with DNA grooves and protein-DNA charge matching often drive the complex formation. Protein structures and their DNA recognition domains are extremely diverse that makes it hard to establish some universal rules of DNA-protein recognition. Several types of interactions can contribute to protein-DNA binding, with the ES and HB contacts being often the dominant ones.

The ES forces are known to dominate a non-specific binding mode for a number of DNA-protein complexes, e.g., weakly bound lac repressor [179]. DNA-binding domains of many relatively small proteins contain positively charged patches that ensure their ES attraction to the DNA. For large protein assemblies, the situation is often quite similar. For RNA Poly II, for instance, a strongly positively charged cleft is identified in the crystal structure along the path taken by DNA-RNA hybrid upon transcription [24]. For ribosomes, the basic residues are also located in protrusions of the structure expected to be involved in binding of tRNA/mRNA during translation [23].

Indeed, Lys⁺ and Arg⁺ residues in DNA-protein complexes are often located only several Å away from DNA phosphates, Fig. 19. ES DNA-protein contacts are however often believed to bear little specificity to DNA sequence [180], merely providing a proximity of proteins to the DNA and allowing more sequence-specific and orientation-dependent HB contacts to recognize HB donors and acceptors inside DNA bases [181]. Below, to confront this opinion, we propose an analytical model for protein-DNA ES recognition. Afterwards, via a systematic computational analysis of PBD structures of protein-DNA complexes, we justify this model for large architectural complexes of pro- and eu-karyotes.

Model of ES recognition. A simple 1D model of DNA-protein recognition based on complementarity of their charge patterns was proposed in Ref. [182]. DNA and protein charge lattices were set commensurate for the cognate site and de-correlated for the rest of the DNA, Fig. 20. In the model, some random charge displacement fields along DNA Δ_n

and protein δ_m mimic a sequence specificity of their charge patterns. This idealized protein is attracted stronger to a particular hom/matching segment on the idealized DNA.

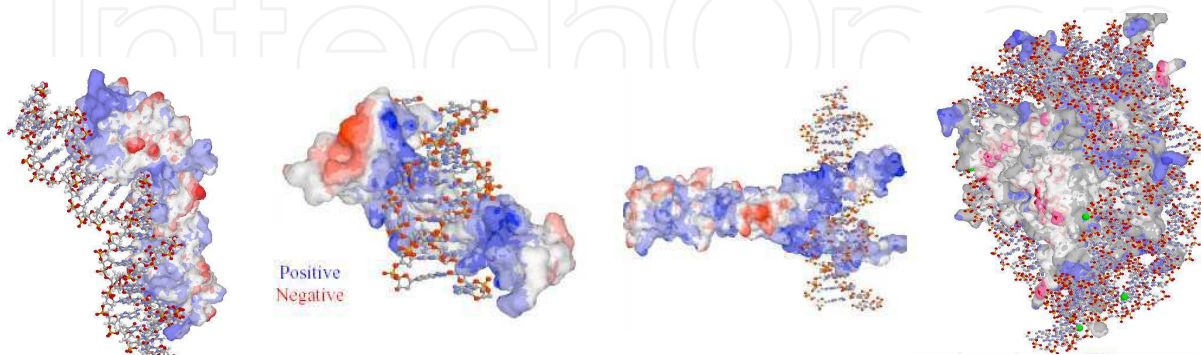


Fig. 19. The distribution of ES potential on DNA-protein complexes of specifically bound lac repressor 1l1m.pdb, zinc finger ZIF268 1aay.pdb, leucine zipper GCN4 1ysa.pdb, and 146 bp NCP 1aoi.pdb (from left to right). The structures are visualized by MDL Chime and Protein Explorer programs, using the PDB files of the complexes. Images are not to scale.

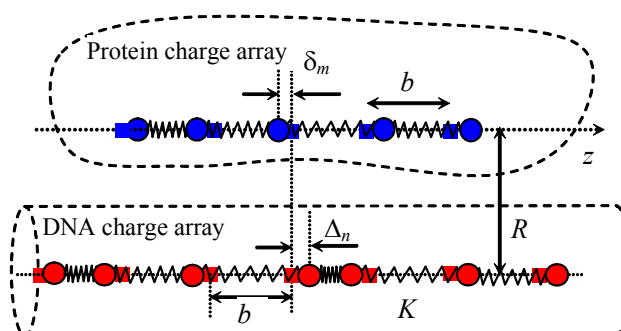


Fig. 20. Schematic 1D-model of “protein-DNA” ES recognition. Charge positions on DNA and protein vary in a random fashion about quasi-periodic positions on 1D lattice.

The average ES recognition energy of a protein to this target site has been derived in the linear PB theory, for random realization of Δ and δ fields. Both long- and short-range order situations for the charges on DNA were investigated (only long-range order results are shown here). For the parameters typical for lac-repressor-like proteins (~ 10 positive charges at $R=1\text{nm}$ from the DNA) the ES recognition well amounts to $\approx 3-10k_B T$ in depth and a couple of nm in width, Fig. 21. Thus, this short-range well cannot serve as “ES funnel” that would direct diffusing proteins from far away on the DNA to this charge-hom binding site. This ES well is thus not expected to facilitate strongly the protein diffusion on DNA, the phenomenon known to take place e.g. for lac- and gal-repressors.

The well depth scales linearly with the number of charges in the hom domain, M . Larger magnitudes of charge deviations from their quasi-periodic positions on the lattice, described

by $\Omega^2 = \langle \Delta_n^2 \rangle + \langle \delta_m^2 \rangle$, also make the well deeper. At zero [salt], the well depth drops as $\propto 1/R^3$ with protein-DNA separation R , while in electrolyte the decay is exponential, $\propto \exp[-R/\lambda_D]$. For weak charge fluctuations in no-salt limit the model returns an elegant expression for the average ES recognition energy well

$$\Delta E(\Delta z) = -\frac{k_B T l_B M \Omega^2 \varepsilon}{2 \varepsilon_c} \frac{R^2 - 2 \Delta z^2}{(R^2 + \Delta z^2)^{5/2}} \quad (6)$$

Here Δz is the mutual protein-DNA sliding distance with respect to the position of complete DNA and protein homology overlap at $\Delta z=0$, see Fig. 21. The charges are assumed to interact through a weakly-polarizable low-dielectric medium between DNA and protein, with the dielectric constant of $\varepsilon_c = 2$.

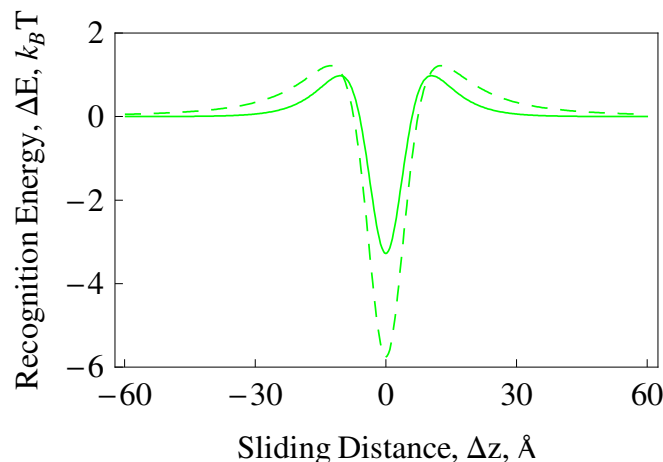


Fig. 21. ES recognition energy well upon sliding of a 1D “protein” over 1D DNA lattice. Parameters: $M=11$ charges in the hom region, $R=10\text{\AA}$, $\Omega^2 = 2 \text{\AA}^2$. The dashed curve is zero-salt limit, the solid curve describes a reduced ES recognition at $1/\kappa = 7 \text{\AA}$.

In this 1D model, the recognition well is accompanied by *energetic barriers*, both for the exact solution and simplistic expression in Eq. 6. The barriers disappear when charge displacements perpendicular to the DNA-protein plane are also taken into account. A generalization of this 1D model for protein and DNA charge displacements for 2D and 3D is more realistic, but only computationally feasible. Also note that some specific, not fully random displacement fields Δ and δ , can mimic charge patterns on a particular DNA sequence and for a given protein. Protein-DNA ES recognition well then resembles DNA-DNA barrier-free ES hom recognition well, sketched in Fig. 16. The calculation of DNA-protein ES recognition is methodologically similar to that for DNA-DNA recognition funnel, Fig. 16.

Let us consider one physical implication of this ES recognition. We have calculated [182] that this well is capable to slow down the protein diffusion, provoking protein trapping for $\sim \mu\text{s}$ -ms near this hom site on DNA. This time is long enough to allow some conformational changes in the protein structure (domain motions, rotation of side-chains, allosteric transition, etc.). Various protein conformation being sampled might trigger a stronger (chemical or HB) protein binding to this particular DNA fragment.

Our hypothesis is thus a *two-step* mechanism of recognition for some proteins. First, a DNA-binding protein scans the ES surface of DNA for a charge-complementary site. In this “searching” mode, the protein structure is flexible and adaptable to the pattern of interaction sites on DNA. When a commensurate DNA fragment is found, some interaction-induced folding solidifies the protein structure, switching it into the “binding” mode that enables stronger and more specific contacts with the DNA. Cumulative ES and HB contacts rigidify the protein structure and give rise to formation of specifically bound DNA-protein complexes.

This kind of hot-spot two-step recognition mechanism is pretty common in structural molecular biology, both for protein-DNA and protein-protein complexes. For the latter, the two-step docking directs the assembly pathway into the native structure by “anchoring” of a shape-complementary relatively rigid “key” domain of one protein into a “lock” domain in the surface of another protein [183]. This process is accompanied by a large burial of solvent accessible surface area and this water release amplifies further docking of proteins into a tight complex.

Analysis of PDB structures. To justify the analytical predictions above, the detailed analysis of PDB structures of different classes of proteins in their complexes with the DNA has been performed. The distribution of NH_2^+ groups on Arginine⁺ and Lysine⁺ residues in DNA-binding domains of DNA-protein complexes has been examined [184]. In particular, large structural complexes were studied: the NCPs of eukaryotes and architectural proteins of prokaryotes, both involving extensive DNA wrapping around the basic protein cores and featuring mainly ES mode of binding. A home-written Mathematica 6 computer code was used for extracting the coordinates of DNA phosphates PO_4^- and protein's N^+ and O^- atoms on the charged amino acids from the PDB files. We could analyse the distances from N^+ atoms on Arg⁺ and Lys⁺ that are within $\approx 7\text{\AA}$ from the closest (s_1) and next closest (s_2) DNA phosphates on the same DNA strand, see Fig. 22. The statistics of ES contacts and salt bridges in these DNA-protein complexes has thus been restored. Smaller cut-off distances of 3-5 \AA can also be used, to minimize the contributions of charges across the narrow DNA groove. Note that fluctuation-induced uncertainties in positions of protein charges in crystals of many DNA-protein complexes are often $\sim 1\text{-}2\text{\AA}$. This is much smaller than the relevant periodicity in the system, the phosphate-phosphate separation along the DNA helical strand, $s_{ph} \approx 7\text{\AA}$.

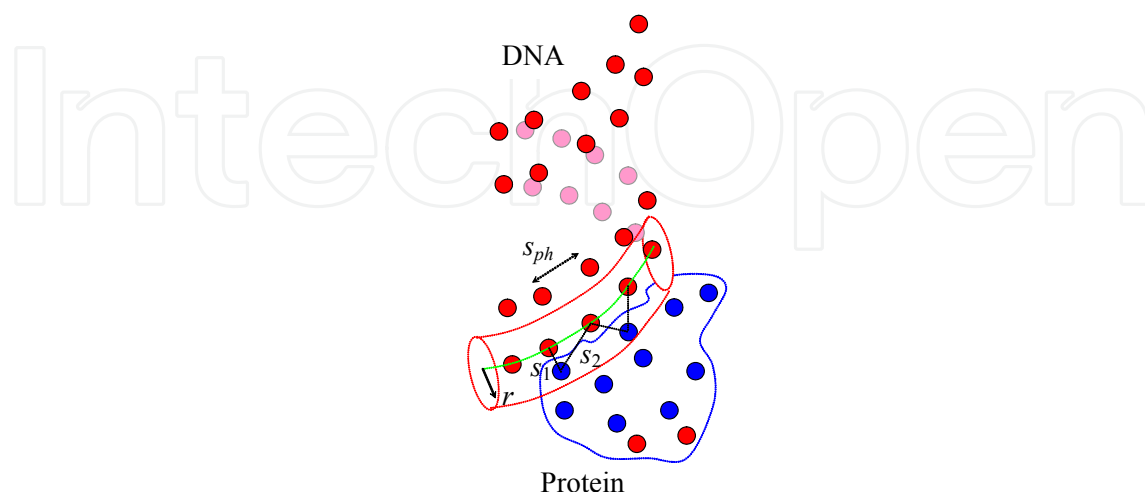


Fig. 22. Definition of $s_{1,2}$ distances for the protein positive charges (in blue) which are closer than $r \sim l_B \approx 7\text{\AA}$ to the negative DNA phosphates (red helix).

For the NCPs, the histone positive charges are mainly localized in the outer “ring” of the octamer, close to the wrapped DNA, see Fig. 19d, with Asp⁻ and Glu⁻ acids being rather inside the core, further away from the DNA. Our analysis demonstrates that N⁺ atoms on Arg⁺ and Lys⁺ track the positions of *individual* DNA phosphates, as visualized in the histogram $s_1 - s_2$ for all N⁺ charges in DNA vicinity, Fig. 23. The *bimodal distributions* were detected both for individual NCPs (a good statistics can be achieved for a single particle) and for the entire family of 146 bp long complexes [184]. This indicates that N⁺ on Lys and Arg are encountered measurably more often close to one of the neighboring DNA phosphates than between the two, maximizing the ES attraction to DNA. As the structure and positions of DNA phosphates strongly correlate to DNA bp sequence [52], this detected “charge tracking” for DNA sequences wrapped in NCPs yields sequence-specific ES DNA-protein forces. This supports our model hypothesis above about commensurate charge lattices on DNA target sequence and on the protein. This fact can contribute to NCP positioning on genomic DNAs, interfering with the mechanism of sequence-specific DNA bendability believed to govern this process [185]. A similar bimodal distribution was obtained for prokaryotic NCP analogs (not shown) [184].

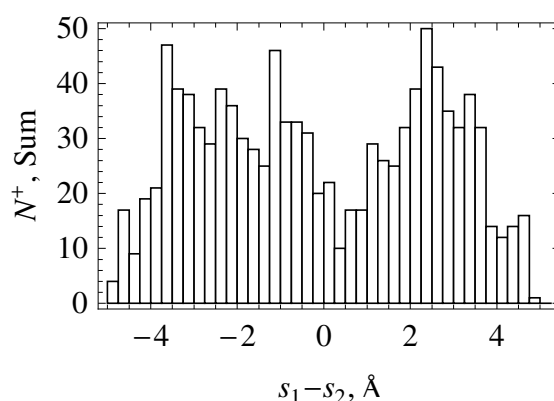


Fig. 23. A bimodal distribution of $s_1 - s_2$ distances for 14 NCP complexes. It indicates the ES recognition of individual DNA phosphates by the closest N⁺ atoms on Arg and Lys basic residues of the histone core proteins.

The specificity of ES binding of Arg and Lys of core histones into the DNA grooves on NCPs has recently been examined by other groups too [186]. The ES-directed localization of Arg⁺ in the minor grooves in AT-rich DNA regions was confirmed for NCPs in Ref. [187]. These studies emphasize that for DNA sequences wrapped in NCPs the AT-tracts have particularly narrow minor grooves that offers “attractive” sites for Arg⁺ and Lys⁺ binding every time the DNA minor groove faces the histone octamer. Arg was claimed to be preferred over Lys in the DNA minor grooves because of a lower self-energy cost to remove a larger guanidinium group of Arg⁺ from its hydrated state in solution. The reason is the Born ES self-energy that scales inversely proportional with the “ion” radius.

Being valid for large structural complexes, the ES complementarity model fails for small DNA-protein complexes, with the standard simple motifs of DNA recognition (e.g., helix-turn-helix, zinc finger, leucine zipper). For a large set of small proteins from these families, we could not detect any statistical preference in distribution of Lys and Arg close to DNA phosphates [184]. To make a more definite conclusion, some redundancy in protein

structures is to be excluded and a grouping into smaller, more specific protein sub-families is to be performed.

A tentative explanation is however as follows. For large complexes, with ~30-100 ES DNA-protein contacts, the ES energy gain being ES-commensurate can reach $\sim 10-30k_B T$ and proteins appear to utilize it for sequence-specific binding to DNA. For small proteins, with only ~3-10 ES contacts and much weaker ES binding, other interactions (such as HBs) are likely to direct the recognition of specific DNA sequences in complexes.

Note that DNA-protein ES commensurability for NCPs and their prokaryotic analogs resembles a *zipper-like* positioning of positive and negative amino acids along interfaces of many protein-protein complexes [18,188]. For the latter, despite hydrophobic residues often dominate the overall binding affinity, these non-charged amino acids might be too abundant to ensure a proper degree of the binding specificity. The latter might stem from *charge patchiness* and propensity of HB formation between the residues along the contact surface of the bound proteins [189]. Analogously, for DNA-DNA interactions, overviewed in Sec. 2, we have seen that DNA-DNA attraction is only possible for entirely commensurate or hom sequences, for which *charge zipper motif* is realized. All these similarities for protein-DNA, protein-protein, and DNA-DNA interactions reflect different aspects of the universal principle of ES complementarity in structural molecular biology.

Challenges and Perspectives. Several issues of description of biophysics of DNA-protein interactions challenge future theoretical developments. First, the computational analysis of PDB data presented above provides us only with a *statistical preference* of distribution of protein charges in DNA proximity. To evaluate the ES binding energies of DNA-protein complexes, one needs to speculate about the value of the dielectric constant ϵ_c in spaces between DNA and protein. Because of dielectric saturation effects in confined/hydrated water molecules on the charged objects [190], its value can vary widely, $\epsilon_c \sim 2\div 30$ [11,12]. So does the ES interaction energy [191]. Another important ES issue is the charged state of ionizable protein residues in a particular neighborhood in DNA-protein complexes (e.g., Hist), with their pK_a value being affected by local ES potential, geometrical shape of the protein surface, [salt], local dielectric permittivity, etc. [11,192].

Non-ES van der Waals and HB contacts, as well as the entropic terms associated with water release and counterion evaporation upon protein-DNA binding, are to be quantified in the future models as well. To make unambiguous conclusion about the mechanism of binding specificity for a given DNA-protein complex, the ES preference of Arg/Lys positioning with respect to DNA phosphates has to be supplemented by the analysis of HB formation propensity between the protein residues and DNA bases [181]. Also, one has to keep in mind that the protein (and DNA) structure visualized by x-rays in crystals exposed to special crystallization buffers [193] might measurably differ from real structures stable at physiological conditions.

There exists an opinion in the literature that ES contacts of charged residues in protein-DNA complexes [4] and along protein-protein interfaces [11] might (somewhat counter-intuitively) *destabilize instead of stabilize* their binding. The argument goes as follows. The release of ES-profitable structured water shells around the constituents often accompanies

DNA-protein complex formation [4,194]. And, it is possible that protein and DNA charged groups complexed together via ES attraction do not fully compensate for the energetic losses upon their “ES desolvation”. The latter depends crucially on the ϵ -value assigned to the protein and its immediate vicinity. For DNA-protein complexes, the entropic effects of condensed cations released from the DNA, with the number defined by the slope of $\log[\text{binding constant}]$ on $\log[\text{salt}]$, are often presented as the main *driving force* for the complexation. Here, the situation is rather similar to counterion release from DNA-(CL membrane) complexes, Sec. 4. In both cases, we however tend to think that the direct ES attraction between the oppositely charged components of the system governs/directs the complex formation, while the entropic free energy gain due to the release of condensed counterions accompanies this process.

11. Conclusions and outlook

In this chapter, we focused on recent developments and new viewpoints on ES effects for a number of biological DNA-related systems. Several experimental achievements and DNA-related phenomena discovered in the last years have been overviewed, which challenge both theoretical and computational modeling. Some analytical insights from our recent studies are discussed, which uncover general principles behind charge-mediated DNA-DNA, NCP-NCP, and DNA-protein interactions. We aimed at describing macroscopic effects having their possible origin in ES interactions as well as at trying to establish correlations between the structure of the system components and their function. The advanced theoretical and computational approaches developed in our studies on DNA-DNA, DNA-membrane and DNA-proteins interactions can find their applications in biotechnology and nano-engineering.

The PE models for DNA and available structure information for the proteins have been applied to some nano-technology applications, the principles of bio-molecular DNA-protein recognition, and self-assembly. Despite inherent limitations of the mean-field PB-like theories applied to the DNA, the approaches developed often enabled us to rationalize the structural properties of the system as dictated by intermolecular forces. The conceptual framework proposed in the chapter allows us to anticipate the physical effects in these DNA-related systems that are still too large for modern *ab initio* computer simulations. Clearly, more work is to be done to achieve a quantitative understanding of these complex phenomena. In particular, the physical properties of inter-connected NCPs in 30 nm chromatin fibers and DNA packaging inside bacteriophages feature a number of important biological details to be incorporated in future theoretical models. Another area is ES effects in protein-mediated loop formation in DNA [195], DNA plectonemes [196,197] and cyclization [198], as well as DNA wrapping in NCPs [199]. These interesting phenomena are however beyond the scope of this contribution.

One hot and intriguing domain of our ES-related biological research is DNA packaging inside viral capsids and self-assembly of viral shells from the capsid proteins [27]. Both processes are highly sensitive to salt conditions that control protein-protein and DNA-DNA ES forces. We argue here that the accurate physical description of DNA compactification inside viral shells demands the application of all theories and models presented in the main text. Let us list the effects one by one.

Many ds-DNA bacteriophages pack their DNA in a very dense and well-organized fashion [200,201,202]. DNA densities can reach $R \approx 23\text{-}28 \text{ \AA}$ between DNA axes, creating osmotic pressures of up to $\sim 50 \text{ atm}$ inside the shells [203,204,205]. At such DNA densities, the effects of DNA helical structure onto DNA-DNA ES forces are going to be extremely pronounced, see

Fig. 24. These effects have been however largely neglected in the existing theories of DNA compaction in ds DNA viruses.

As the capsids of some ds-DNA viruses are penetrable for small ions [40], the presence of di- and tri-valent cations in the solution can render DNA-DNA ES forces inside the capsids more attractive [212]. This will ease DNA packaging into and inhibit the DNA ejection from such capsids. Indeed, only 1 mM of spermine⁴⁺ in the buffer blocks nearly 90% of DNA inside the λ -phage capsids [206]. The counterion-mediated DNA-DNA attraction inside viral capsids is a clear target for our ES interaction theory presented in Sec. 2.

Typical for ds-DNA viruses are the concentric rings of DNA [207,208,209], with the DNA layers that are closer to the viral shell being resolved better by the cryo-EM image reconstruction, see Fig. 24. This corresponds to a coaxial inverse-spool model of DNA packing, with the outer (more ordered) shells of the DNA spool being filled first. Recently, oriented DNA toroids condensed with spermine⁴⁺ inside T4 phages [75] and DNA “domain-wall” transitions upon DNA ejection from T5 phages [210] have been clearly visualized by cryo-EM. The interaction of toroidal DNA condensates overviewed in Sec. 3 with the confining protein shells of the capsid is a proper model to describe this “deformed toroid” conformation of spooling DNA [76]. Cholesteric ES effects, see Sec. 5, onto the DNA packing properties were also argued to be important for many ds DNA viruses. Lastly, the pauses in DNA packaging and ejection caused by necessary rearrangements of DNA spool [211] might stem from ES friction between the densely packed DNA layers inside the capsid, see Sec. 8.

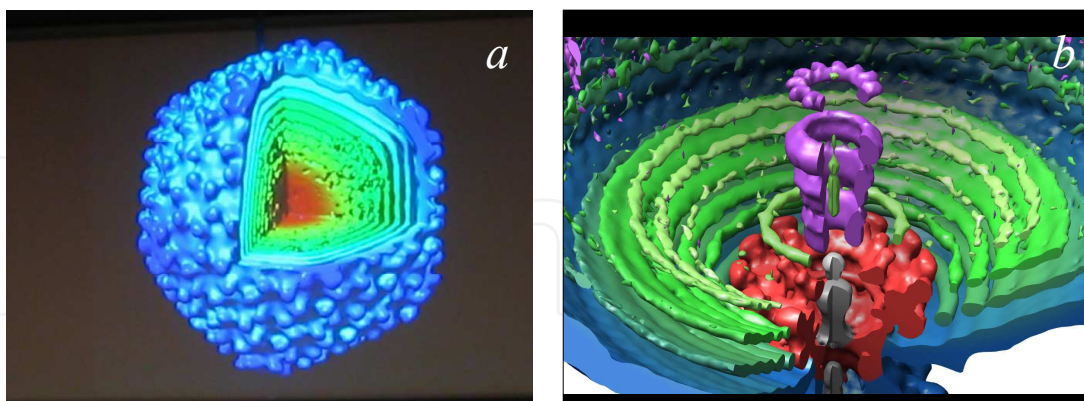


Fig. 24. The result of 3D reconstruction of cryo-EM images with DNA layers inside P22 virus (a), with DNA layers being more ordered near the portal region (b, bottom). Images are the courtesy of J. Johnson.

12. Acknowledgment

I am thankful to T. Bellini, R. Everaers, N. Kleckner, A. Kolomeisky, A. Kornyshev, D. Lee, S. Leikin, S. Malinin, W. Olson, E. Petrov, A. Poghosian, M. Prentiss, E. Starostin, R. Winkler,

G. Wuite and G. Zanchetta for many stimulating discussions and scientific correspondence. Without a constant help and encouragement of my collaborators (see joint publications below) this chapter would not be possible. A part of this work was supported by the German Research Foundation, DFG Grants CH 707/5-1 and CH 707/2-2. Because of space restrictions, only a small fraction of relevant studies has been cited in the text (my apologies to the authors which could not be mentioned).

13. References

- [1] W. M. Gelbart et al., *Phys. Today*, 53 38 (2000).
- [2] S. McLaughlin, *Annu. Rev. Biophys. Biophys. Chem* 18 113 (1989).
- [3] C. G. Kalodimos et al., *Science*, 305 386 (2004).
- [4] B. Honig and A. Nicholls, *Science*, 268 1144 (1995).
- [5] K. Luger et al., *Nature*, 389 251 (1997).
- [6] T. J. Richmond and C. Davey, *Nature*, 423 145 (2003).
- [7] J. H. Morais-Cabral et al., *Nature*, 414 37 (2001).
- [8] G. C. L. Wong and L. Pollack, *Annu. Rev. Phys. Chem.*, 61 171 (2010).
- [9] A. A. Kornyshev et al., *Rev. Mod. Phys.*, 79 943 (2007).
- [10] S. J. Chen, *Ann. Rev. Biophys.*, 37 197 (2008).
- [11] A. Warshel and T. S. Russell, *Quart. Rev. Biophys.*, 17 283 (1984).
- [12] F. B. Sheinerman et al., *Curr. Opin. Struct. Biol.*, 10 153 (2000).
- [13] A. Warshel et al., *Biochim. Biophys. Acta*, 1764 1647 (2006).
- [14] R. P. Rand, *Ann. Rev. Biophys. Bioeng.*, 10 277 (1981).
- [15] G. Cevc, *Biochim. Biophys. Acta*, 1031 311 (1990).
- [16] R. Messina, *J. Phys.: Cond. Matter*, 21 113102 (2009).
- [17] P. H. von Hippel, *Science*, 305 350 (2004).
- [18] A. J. McCoy et al., *J. Mol. Biol.*, 268 570 (1997).
- [19] H. Schiessel, *J. Phys.: Cond. Matt.*, 15 R699 (2003).
- [20] C. L. Woodcock and R. P. Ghosh, *Cold Spring Harb. Perspect. Biol.*, 2 a000596 (2010).
- [21] C. M. Knobler and W. M. Gelbart, *Ann. Rev. Phys. Chem.*, 60 367 (2009).
- [22] D. E. Draper, *Biophys. J.*, 95 5489 (2008).
- [23] N. A. Baker et al., *PNAS*, 98 10037 (2001).
- [24] R. D. Kornberg et al., *Science*, 292 1863 (2001).
- [25] V. A. Parsegian and D. Gingell, *J. Adhesion*, 4 283 (1972).
- [26] A. A. Kornyshev and S. Leikin, *J. Chem. Phys.*, 107 3656 (1997).
- [27] A. G. Cherstvy, *Phys. Chem. Chem. Phys.*, 13 9942 (2011).
- [28] G. S. Manning, *Q. Rev. Biophys.*, 11 179 (1978).
- [29] R. M. M. Smeets, *Nano Lett.*, 6 89 (2006).
- [30] S. van Dorp et al., *Nature Physics*, 5 347 (2009).
- [31] A. G. Cherstvy, *J. Chem. Phys.*, 123 116101 (2005).
- [32] J. DeRouchey et al., *Biophys. J.* 99 2608 (2010).
- [33] D. C. Rau and V. A. Parsegian, *Science*, 249 1278 (1990).
- [34] S. Leikin et al., *PNAS*, 91 276 (1994).
- [35] V. A. Parsegian et al., *PNAS*, 76 2750 (1979).

- [36] D. C. Rau and V. A. Parsegian, *Biophys. J.*, 61 260 (1992); *ibid.*, 61 272 (1992).
- [37] B. A. Todd et al., *Biophys. J.*, 94 4775 (2008).
- [38] H. H. Strey et al., *Phys. Rev. E*, 59 999 (1999).
- [39] P. Shah and E. Swiatlo, *Molec. Microbiol.*, 68 4 (2008).
- [40] B. N. Ames and D. T. Dubin, *J. Biol. Chem.*, 235 769 (1960).
- [41] M. Kanduč et al., *Soft Matter*, 5 868 (2009).
- [42] V. B. Teif and K. Bohinc, *Progr. Biophys. Mol. Biol.*, 105 208 (2011).
- [43] I. Rouzina and V. A. Bloomfield, *J. Phys. Chem.*, 100 9977 (1996).
- [44] H. Boroudjerdi et al., *Phys. Rep.*, 416 129 (2005).
- [45] Y. Levin, *Rep. Prog. Phys.*, 65 1577 (2002).
- [46] N. Gronbech-Jensen et al., *Phys. Rev. Lett.*, 78, 2477 (1997).
- [47] E. Allahyarov et al., *Phys. Rev. E*, 69 041904 (2004).
- [48] M. Deserno et al., *Macromol.*, 36 249 (2003).
- [49] B. Luan and A. Aksimentiev, *JACS*, 130 15754 (2008).
- [50] A. A. Kornyshev and S. Leikin, *Phys. Rev. Lett.*, 82 4138 (1999).
- [51] A. A. Kornyshev and S. Leikin, *PNAS*, 95 13579 (1998).
- [52] W. K. Olson et al., *PNAS*, 95 11163 (1998).
- [53] A. A. Kornyshev and S. Leikin, *Phys. Rev. Lett.*, 86 3666 (2001).
- [54] A. G. Cherstvy et al., *J. Phys. Chem. B*, 106 13362 (2002).
- [55] A. G. Cherstvy et al., *J. Phys. Chem. B*, 108 6508 (2004).
- [56] A. A. Kornyshev and A. Wynveen, *Phys. Rev. E*, 69 041905 (2004).
- [57] A. Wynveen et al., *Nucl. Acid Res.*, 36 5540 (2008).
- [58] A. A. Kornyshev and S. Leikin, *Phys. Rev. Lett.*, 84 2537 (2000).
- [59] A. A. Kornyshev et al., *Eur. Phys. J. E*, 7 83 (2002).
- [60] A. Wynveen et al., *Eur. Phys. J. E*, 16 303 (2005).
- [61] H. M. Harreis et al., *Phys. Rev. Lett.*, 89 018303 (2002).
- [62] A. A. Kornyshev et al., *Phys. Rev. Lett.*, 95 148102 (2005).
- [63] H. H. Strey et al., *Phys. Rev. Lett.*, 84 3105 (2000).
- [64] D. J. Lee et al., *J. Phys. Condens. Matter*, 22 072202 (2010).
- [65] D. J. Lee et al., *J. Phys. Chem. B*, 114 11668 (2010).
- [66] D. J. Lee, *J. Phys. Condens. Matter*, 22 414101 (2010).
- [67] A. A. Kornyshev, *Phys. Chem. Chem. Phys.*, 12 12352 (2010).
- [68] H. H. Strey et al., *Phys. Rev. Lett.*, 78 895 (1997).
- [69] G. M. Grason, *EPL*, 83 58003 (2008).
- [70] A. G. Cherstvy, PhD Thesis, Düsseldorf University, 2002.
- [71] V. A. Bloomfield, *Curr. Opin. Struct. Biol.*, 6 334 (1996).
- [72] S. Levin-Zaidman, *Science*, 299 254 (2003).
- [73] J. Englander et al., *J. Bacteriol.*, 186 5973 (2004).
- [74] N. V. Hud et al., *Biochem. Biophys. Res. Comm.*, 193 1347 (1993).
- [75] A. Leforestier and F. Livolant, *PNAS*, 106 9157 (2009).
- [76] A. Leforestier et al., *Biophys. J.*, 100 2209 (2011).
- [77] N. V. Hud and K. N. Downing, *PNAS*, 98 14925 (2001).
- [78] S. M. Douglas et al., *Nature*, 459 414 (2009).
- [79] H. Dietz et al., *Science*, 325 725 (2009).

- [80] A. G. Cherstvy, *J. Phys.: Cond. Matter*, 17 1363 (2005).
- [81] C. G. Baumann et al., *PNAS*, 94 6185 (1997).
- [82] J. P. Peters and L. J. Maher III, *Quart. Rev. Biophys.*, 43 23 (2010).
- [83] J. Ubbink and T. Odijk, *EPL*, 33 353 (1996).
- [84] J. Kindt et al., *PNAS*, 98 13671 (2001).
- [85] I. M. Kulic et al., *EPL*, 67 418 (2004).
- [86] N. V. Hud et al., *PNAS*, 92 3581 (1995).
- [87] B. van den Broek et al., *Biophys. J.*, 98 1902 (2010).
- [88] C. Battle et al., *Phys. Rev. E*, 80 031917 (2009).
- [89] Y. Sh. Mamasakhlisov et al., *Phys. Rev. E*, 80 031915 (2009).
- [90] G. G. Pereira and D. R. M. Williams, *Biophys. J.*, 80 161 (2001).
- [91] C. Herold et al., *Phys. Rev. Lett.*, 104 148102 (2010).
- [92] E. Petrov and A. G. Cherstvy, work in preparation.
- [93] J. O. Raedler et al., *Science*, 275 810 (1997).
- [94] G. C. L. Wong et al., *Science*, 288 2035 (2000).
- [95] U. Raviv et al., *PNAS*, 102 11167 (2005).
- [96] L. Tang et al., *Nature Materials*, 3 615 (2004).
- [97] G. Martini and L. Ciani, *Phys. Chem. Chem. Phys.*, 11 211 (2009).
- [98] K. K. Ewert et al., *Expert Opin. Biol. Therapy*, 55 33 (2005).
- [99] I. Koltover et al., *Science*, 281 78 (1998).
- [100] G. Caracciolo et al., *J. Phys. Chem. B*, 114 2028 (2010).
- [101] K. Wagner et al., *Langmuir*, 16 303 (2000).
- [102] D. Harries et al., *Biophys. J.*, 75 159 (1998).
- [103] S. May et al., *Biophys. J.*, 78 1681 (2000).
- [104] D. Harries et al., *Coll. Surf. A*, 208 41 (2002).
- [105] O. Farago et al., *Phys. Rev. Lett.*, 96 018102 (2006).
- [106] L. Gao et al., *J. Phys. Chem. B*, 114 7261 (2010).
- [107] G. Tresset and Y. Lansac, *J. Phys. Chem. Lett.*, 2 41 (2011).
- [108] C. Fleck et al., *Biophys. J.*, 82 76 (2002).
- [109] H. Schiessel and H. Aranda-Espinoza, *Eur. Phys. J. E*, 5 499 (2001).
- [110] A. G. Cherstvy, *J. Phys. Chem. B*, 111 12933 (2007).
- [111] T. Salditt et al., *Phys. Rev. E*, 58 889 (1998).
- [112] R. Menes et al., *Eur. Phys. J. E*, 1 345 (2000).
- [113] I. Koltover et al., *PNAS*, 97 14046 (2000).
- [114] E. Raspaud et al., *Biophys. J.*, 88 392 (2005).
- [115] Y. S. Tarahovsky et al., *Biophys. J.*, 87 1054 (2004).
- [116] A. Leforestier and F. Livolant, *Biophys. J.*, 65 56 (1993).
- [117] A. D. Rey, *Soft Matter*, 6 3402 (2010).
- [118] E. Grelet and S. Fraden, *Phys. Rev. Lett.*, 90 198302 (2003).
- [119] L. Rudd et al., *Phys. Chem. Chem. Phys.*, 8 4347 (2006).
- [120] J. Lepault et al., *EMBO J.*, 6 1507 (1987).
- [121] F. Livolant and M. F. Maestre, *Biochem.* 27 3056 (1988).
- [122] N. S. Blanc et al., *J. Struct. Biol.*, 134 76 (2001).
- [123] C. B. Stanley et al., *Biophys. J.*, 89 2552 (2005).

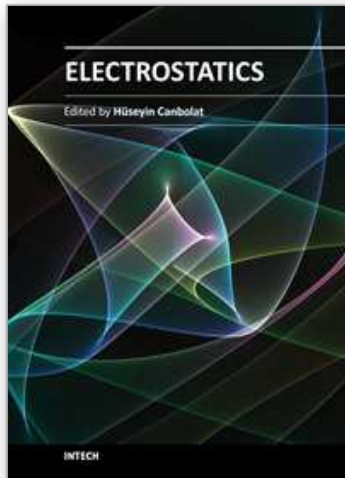
- [124] J. Pelta et al., *Biophys. J.*, 71 48 (1996).
- [125] A. A. Kornyshev and S. Leikin, *Phys. Rev. E*, 62 2576 (2000).
- [126] J. P. Straley, *Phys. Rev. A*, 14 1835 (1976).
- [127] F. Tombolato and A. Ferrarini, *J. Chem. Phys.*, 122 054908 (2005).
- [128] A. G. Cherstvy, *J. Phys. Chem. B*, 112 12585 (2008).
- [129] F. G. Donnan, *Chem. Rev.*, 1 73 (1924).
- [130] G. Zanchetta et al., *PNAS*, 107 17497 (2010).
- [131] M. Nakata et al., *Science*, 318 1276 (2007).
- [132] G. Zanchetta et al., *PNAS*, 105 1111 (2008).
- [133] P. Varnai and Y. Timsit, *Nucl. Acid Res.*, 38 4163 (2010).
- [134] E. Frezza et al., *Soft Matter*, 7 9291 (2011).
- [135] A. Goldar et al., *J. Phys. Cond. Matter*, 20 035102 (2008).
- [136] C. L. Woodcock et al., *Chromosome Res.*, 14 17 (2006).
- [137] J. T. Finch and A. Klug, *PNAS*, 73 1897 (1976).
- [138] T. Schalch et al., *Nature*, 436 138 (2005).
- [139] P. J. J. Robinson et al, *PNAS*, 103 6506 (2006).
- [140] K. Luger and T. J. Richmond, *Curr. Opin. Struct. Biol.*, 8 33 (1998).
- [141] C. L. White et al., *EMBO J.*, 20 5207 (2001).
- [142] Y. Cui and C. Bustamante, *PNAS*, 97 127 (2000).
- [143] M. Kruithof et al., *Nat. Struct. Mol. Biol.*, 16 534 (2009).
- [144] S. Mangenot et al., *Biophys. J.*, 84 2570 (2003).
- [145] A. Leforestier et al., *Biophys. J.*, 81 2414 (2001).
- [146] K. Luger et al., *PNAS*, 101 6864 (2004).
- [147] A. G. Cherstvy and R. Everaers, *J. Phys. Cond. Mat.*, 18 11429 (2006).
- [148] A. A. Kornyshev and A. Wynveen, *PNAS*, 106 4683 (2009).
- [149] A. Barzel and M. Kupiec, *Nature Rev. Gen.*, 9 27 (2008).
- [150] A. Weiner et al., *Nature Rev. Microbiol.*, 7 748 (2009).
- [151] W. K. Olson and V. B. Zhurkin, *Curr. Opin. Struct. Biol.*, 10 286 (2000).
- [152] A. A. Gorin et al., *J. Mol. Biol.*, 247 34 (1995).
- [153] B. S. Singer et al., *Cell*, 31 25 (1982).
- [154] B. M. Weiner and N. Kleckner, *Cell*, 77 977 (1994).
- [155] S. Inoue et al., *Biochemistry*, 46 164 (2007).
- [156] G. S. Baldwin et al., *J. Phys. Chem B*, 112 1060 (2008).
- [157] M. Prentiss et al., *PNAS*, 106 19824 (2009).
- [158] N. Kleckner, *PNAS*, 93 8167 (1996).
- [159] A. G. Cherstvy, *J. Mol. Recogn.*, 24 283 (2011).
- [160] M. Urbakh and E. Meyer, *Nature Mat.*, 9 8 (2010).
- [161] I. Barel et al., *Phys. Rev. Lett.*, 104 066104 (2010).
- [162] N. Clauvelin et al., *Biophys. J.*, 96 3716 (2009).
- [163] R. T. Dame et al., *Nature*, 444 387 (2006).
- [164] M. C. Noom et al., *Nature Methods*, 4 1031 (2007).
- [165] A. G. Cherstvy, *J. Phys. Chem. B*, 113 5350 (2009).
- [166] A. G. Cherstvy and R. G. Winkler, *J. Chem. Phys.*, 120 9394 (2004).

- [167] D. Poland and H.A. Scheraga, *Theory of Helix-Coil Transition in Biopolymers*, Academic Press, New York (1970).
- [168] M. Peyrard and A. R. Bishop, *Phys. Rev. Lett.*, 62 2755 (1989).
- [169] D. Jost and R. Everaers, *Biophys. J.*, 96 1056 (2009).
- [170] A. G. Cherstvy and A. A. Kornyshev, *J. Phys. Chem. B*, 109 13024 (2005).
- [171] D. Grasso et al., *Liquid Cryst.*, 9 299 (1991).
- [172] R. Jin et al., *JACS*, 125 1643 (2003).
- [173] H. Long et al., *J. Phys. Chem. B*, 110 2918 (2006).
- [174] O.-S. Lee et al., *J. Phys. Chem. Lett.*, 1 1781 (2010).
- [175] C. Schildkraut and S. Lifson, *Biopolym.*, 3 195 (1965).
- [176] M. Peyrard et al., *Phys. Rev. E*, 83 061923 (2011).
- [177] A. Poghossian et al., *Sens. & Actuators B*, 111-112 470 (2005).
- [178] A. Poghossian et al., submitted, (2011).
- [179] C. G. Kalodimos, et al., *Science*, 305 386 (2004).
- [180] P. H. von Hippel and O. G. Berg, *PNAS*, 83 1608 (1986).
- [181] N. M. Luscombe et al., *NAR*, 29 2860 (2001).
- [182] A. G. Cherstvy et al., *J. Phys. Chem. B*, 112 4741 (2008).
- [183] D. Rajamani et al., *PNAS*, 101 11287 (2004).
- [184] A. G. Cherstvy, *J. Phys. Chem. B*, 113 4242 (2009).
- [185] E. Segal et al., *Nature*, 442 772 (2006).
- [186] D. Wang et al., *J. Biomol. Struct. Dyn.*, 27 843 (2010).
- [187] B. Honig et al., *Nature*, 461 1248 (2009).
- [188] T. Takahashi, *Adv. Biophys.*, 34 41 (1997).
- [189] O. Keksin et al., *J. Mol. Biol.*, 245 1281 (2005).
- [190] C. N. Schutz and A. Warshel, *Proteins*, 44 400 (2001).
- [191] A. T. Fenley et al., *J. Chem. Phys.*, 129 075101 (2008).
- [192] J. Antosiewicz et al., *Biochem.*, 35 7819 (1996).
- [193] R. E. Dickerson et al., *PNAS*, 91 3579 (1994).
- [194] V. K. Misra et al., *Biophys. J.*, 75 2262 (1998).
- [195] A. G. Cherstvy, *Europ. Biophys. J.*, 40 69 (2011).
- [196] A. G. Cherstvy, *J. Biol. Phys.*, 37 227 (2011).
- [197] R. Cortini et al., *Biophys. J.*, 101 875 (2011).
- [198] A. G. Cherstvy, *J. Phys. Chem. B*, 115 4286 (2011).
- [199] A. G. Cherstvy and R. G. Winkler, *J. Phys. Chem. B*, 109 2962 (2005).
- [200] W. C. Earnshaw and S. C. Harrison, *Nature*, 268 598 (1977).
- [201] W. M. Gelbart and C. M. Knobler, *Physics Today*, 61 42 (2008).
- [202] W. M. Gelbart and C. M. Knobler, *Science*, 323 1682 (2009).
- [203] D. E. Smith et al., *Nature*, 413 748 (2001).
- [204] D. N. Fuller et al., *PNAS*, 104 11245 (2007).
- [205] P. Grayson et al., *PNAS*, 104 14652 (2007).
- [206] A. Evilevitch et al., *Biophys. J.*, 94 1110 (2008).
- [207] M. E. Cerritelli et al., *Cell*, 91 271 (1997).
- [208] A. Fokine et al., *PNAS*, 101 6003 (2004).
- [209] J. Johnson et al., *Science*, 312 1791 (2006).

- [210] A. Leforestier and F. Livolant, *J. Mol. Biol.*, 396 384 (2010).
[211] D. Marenduzzo et al., *PNAS*, 106 22269 (2009).
[212] A. Siber et al., *Phys. Chem. Chem. Phys.*, DOI: 10.1039/C1CP22756D

IntechOpen

IntechOpen



Electrostatics

Edited by Dr. Hüseyin Canbolat

ISBN 978-953-51-0239-7

Hard cover, 150 pages

Publisher InTech

Published online 14, March, 2012

Published in print edition March, 2012

In this book, the authors provide state-of-the-art research studies on electrostatic principles or include the electrostatic phenomena as an important factor. The chapters cover diverse subjects, such as biotechnology, bioengineering, actuation of MEMS, measurement and nanoelectronics. Hopefully, the interested readers will benefit from the book in their studies. It is probable that the presented studies will lead the researchers to develop new ideas to conduct their research.

How to reference

In order to correctly reference this scholarly work, feel free to copy and paste the following:

Andrey G. Cherstvy (2012). Electrostatic Interactions in Dense DNA Phases and Protein-DNA Complexes, *Electrostatics*, Dr. Hüseyin Canbolat (Ed.), ISBN: 978-953-51-0239-7, InTech, Available from: <http://www.intechopen.com/books/electrostatics/electrostatic-interactions-in-dense-dna-phases-and-protein-dna-complexes>

INTECH
open science | open minds

InTech Europe

University Campus STeP Ri
Slavka Krautzeka 83/A
51000 Rijeka, Croatia
Phone: +385 (51) 770 447
Fax: +385 (51) 686 166
www.intechopen.com

InTech China

Unit 405, Office Block, Hotel Equatorial Shanghai
No.65, Yan An Road (West), Shanghai, 200040, China
中国上海市延安西路65号上海国际贵都大饭店办公楼405单元
Phone: +86-21-62489820
Fax: +86-21-62489821

© 2012 The Author(s). Licensee IntechOpen. This is an open access article distributed under the terms of the [Creative Commons Attribution 3.0 License](#), which permits unrestricted use, distribution, and reproduction in any medium, provided the original work is properly cited.

IntechOpen

IntechOpen